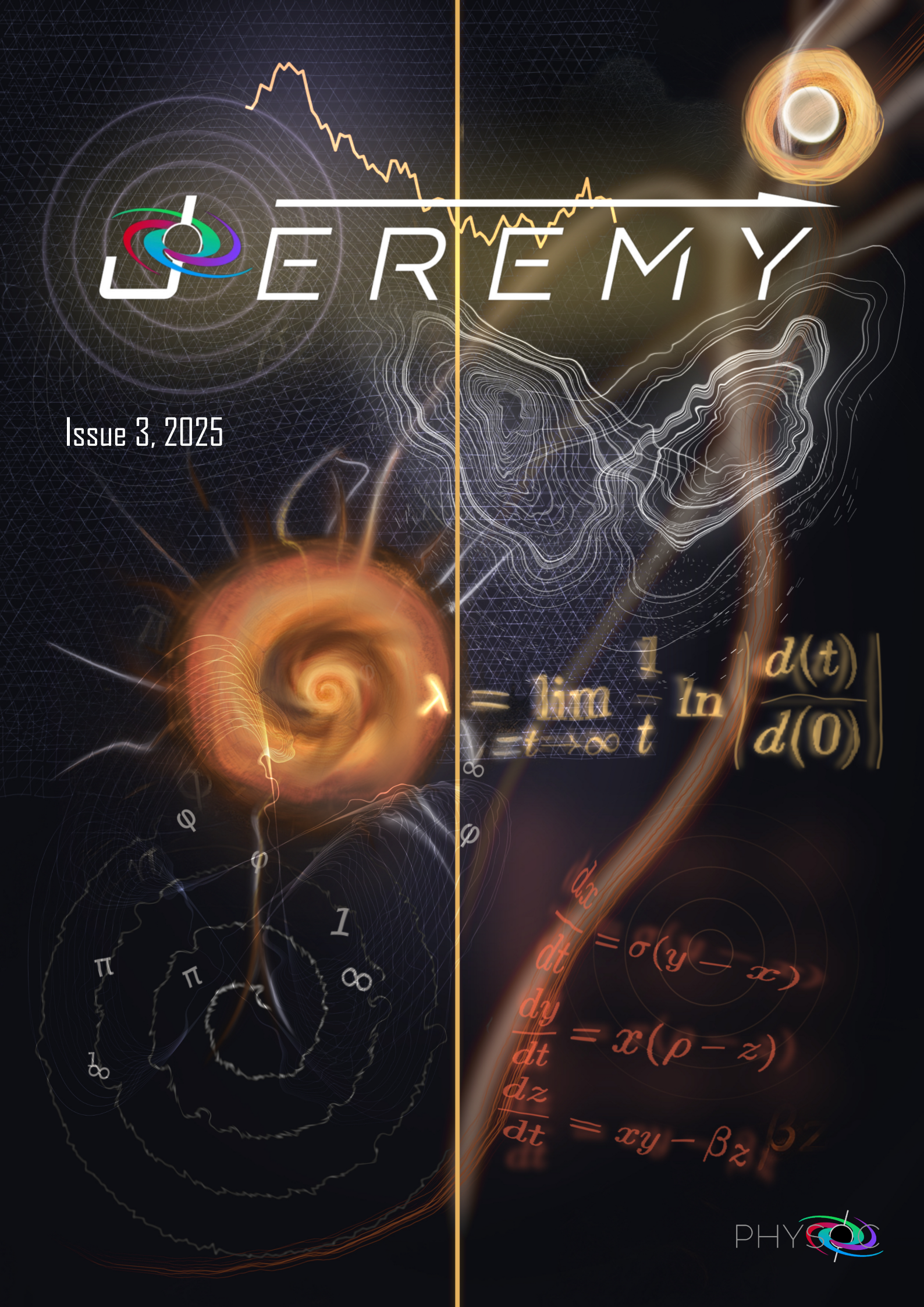
JEREMY
Issue 3, 2025
$\lambda = \lim_{t \to \infty} \frac{1}{t} \ln \left| \frac{d(t)}{d(0)} \right|$
$\frac{dx}{dt} = \sigma(y - x)$
$\frac{dy}{dt} = x(\rho - z)$
$\frac{dz}{dt} = xy - \beta z$
PHYSICS

CHAOS contents

Jeremy Team: Peter Lavilles, Mani Shayestehfar, Stephanie Chen, Aruna Sathyanarayanan Balaprabhavathi, Queenie Pham, Angela Liang, Jude Metcalf, Imasha Fernando, Ho Dieu Bao Nguyen, Raine Li, Lydia Zhang, Toby McErlane, Josh Ferguson, and the rest of the PHYSOC team!

PHYSOC JEREMY

Issue 3, 2025 *The Physics Society Magazine*

Editorial

At first glance, chaos and physics seem like opposing ideas. Physics seeks to understand, to predict, to impose order. Chaos resists all of that; it twists systems away from neat equations and leaves us with outcomes that defy intuition. But within the depths of dynamical systems around us, the intricate dance of planetary objects, the ever-changing weather systems around the globe, and even through something as simple as the movement of masses attached to a string, we find a sort of complexity. One that is deeply sensitive to initial conditions, and the complications that occur when a system involves too many variables. Colloquially, The word "chaos" has a negative ring to it. But in physics, chaos is all around us, and more beautiful than imaginable!

This issue of Jeremy is a bit *chaotic*. We explore this aspect of physics and mathematics, as well as some slightly different articles of course, through the lens of our writers. We start off from the very famous Lorentz attractors, and explore them in areas least expected, such as our hearts. We then take a tangent to a book review, "Inward Bound" by Abraham Pais, which takes us through a bit of physics history. We then regather on how chaotic N-body systems can be computationally modelled with some physical curiosity. If we are still hungry for some more knowledge, we can take a look at the chaos in the neural dynamics of our brains and explore what we call hallucinations! Afterwards, we take a look at how sometimes mathematical rigour can be swept under the rug in physics by investigating the notion of continuity and weird, unintuitive examples of them such as "Cantor's Evil Function"! And finally, we embark on a journey to understand spinors and Hopf fibrations in mathematical detail in what is part 1 out of 2 of this series.

So, do we have a deal? Or are we just another set of particles bouncing unpredictably in phase space, hoping to converge on meaning? Either way, fasten your seatbelts. This issue might be sensitive to initial conditions. Don't blame us if reading one article leads to a spontaneous interest in Chaos theory, Analysis, Complex systems, or philosophical dread. That's just part of the butterfly effect.

Welcome to this beautifully unpredictable rhythm that is *Jeremy*.

The Quote Competition

The winning quotes for this issue are:

> *"The point is, you're not meant to understand what I'm doing"*
>
> - Dr. Wave Ngampruetikorn

Context: A typical lecture in 3rd year condensed matter physics!

> *"And now... we divide by zero"*
>
> - Prof. Florica Cîrstea

Context: A mathematician does, as a mathematician should!

Would you like to publish your work? Whether it is a short and fun blurb, or a full-on scientific paper, or some funny quotes, Jeremy is a place to kick off your scientific ingenuity! Send your submissions to :

jeremy.physoc@gmail.com

Meet the School of Physics

Meet Prof. Zdenka Kuncic! With a love for ancient history and Croatian food, Zdenka has synthesised research across astrophysics and medical imaging. Her current project? Building brain-like devices with true artificial intelligence that sit at the crossroads between order and chaos...

Chaos: Predicting the Unpredictable

From the Weather to the Heart

By Queenie Pham

In everyday language, "chaos" implies the existence of unpredictable or random behaviour. The word usually carries a negative connotation involving undesirable havoc or utter pandemonium, the scale of which ranges from the notorious rush hour traffic in Ho Chi Minh city to the clutter on your bedroom floor.

However, in the realm of physics, chaos is not necessarily undesirable, nor is it random.

Imagine bouncing a tennis ball on a rough slab of concrete. It will bounce around seemingly randomly. Except it isn't random, and if you could map out the movement of the ball across the surface, you could predict where it would land using Newton's fundamental laws of motion. Yet, there will still be tiny differences in the first bounce, caused by subtle variations in the impact angle, mechanical force, clumps or gentle dips in the cement. This will change where the next bounce lands, which likely completely alters the trajectory of the bounces thereafter, rendering the movement of the tennis ball practically unpredictable even though it is merely following simple rules.

For small uncertainties in the initial states of the tennis ball, we observe an exponential increase in the uncertainty of its future states.

The bouncing tennis ball encapsulates the principles of a chaotic system. It is highly sensitive to initial conditions; its motion is deterministic yet irregular - irregular but not random. Moreover, the complex interplay between the ball's rotation, deformation, vertical and horizontal positions give rise to a nonlinear system, where outputs are not linearly proportional to inputs.

For another example of chaos, recall instances of you arriving home drenched when the forecast had anticipated low chances of rainfall. To understand where this uncertainty came from, consider the process of predicting the weather.

Measurements of the air pressure, temperature, humidity, heat transfer, evaporation and condensation of water are collected from satellites and radar observations [1]. This data is fed into mathematical models of the Earth's atmosphere to produce weather forecasts, which are essentially computer simulations that describe the complex interactions between these atmospheric elements [1]. To construct a perfectly accurate forecast, meteorologists would have to know the exact conditions of every single molecule in the global system, and use these as inputs for a cosmic computer model that is the exact mathematical representation of every physical process involved [2]. This is highly unattainable for two reasons. The first is a direct result of Heisenberg's uncertainty principle [1] - we cannot know the exact conditions of a molecule because we cannot be certain of both the velocity and position of an object in the same instant. This demonstrates that our most careful measurements of the atmosphere are only approximations. Furthermore, mathematical models are, at best, a sophisticated rendering of reality. Initial conditions are never known with 100% certainty, and in chaotic systems such as this, any variations in the initial conditions may result in exponentially diverging outputs [1].

Chaos explains why weather predictions can be inaccurate. In fact, most meteorology apps do not display data beyond the next fourteen days because long-term weather forecasting is increasingly inaccurate.

Meteorological models were extensively studied by Edward Lorenz in the 1960s. In one experiment, he simplified the inputs to 0.506 instead of including the next three digits in the original sequence, 0.506127 [3]. From Figure 1, the initial pattern appeared to overlap, however the new sequence eventually diverged, ending up wildly different from the original.

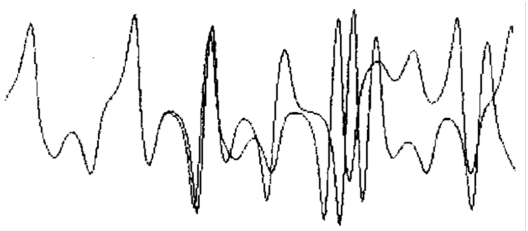

Figure 1: Results from Lorenz's experiment, where two trajectories diverge although starting values differ by only 0.000127. Diagram taken from [3].

In 1963, Lorenz' seminal work on chaos theory culminates with a refined mathematical model that describes atmospheric convection, or any system that exhibits chaotic behaviour. His system consists of three simplified variables, x, y, and z, obeying the differential equations [4]:

$$\frac{dx}{dt} = \sigma(y - x) \tag{1}$$

$$\frac{dy}{dt} = x(\rho - z) \tag{2}$$

$$\frac{dz}{dt} = xy - \beta z \tag{3}$$

The parameter σ represents the Prandtl number, indicating the ratio between momentum and thermal diffusivity through a fluid [4]. The parameter ρ is the Rayleigh number which reveals whether heat transfer is dominated by convection or conduction, and β denotes the relative dimension of the fluid, or more specifically, the ratio of the width to the height of the fluid layer [4].

Through experimentation, Lorenz found that for certain parameters ($\sigma = 10$, $\beta = 8/3$, and $\rho = 28$), the time series for the x, y, and z variables from (1), (2) and (3) depict unpredictable and non-periodic trajectories [5], as shown in Figure 2. By choosing different initial coordinates (x, y, z), Lorenz plotted the curves as functions of time in a three-dimensional space. From Figure 3, it is observed that the solutions never intersect, thus each trajectory commits to infinite solitude, and this divergence rate for similar trajectories is known as the Lyapunov exponent.

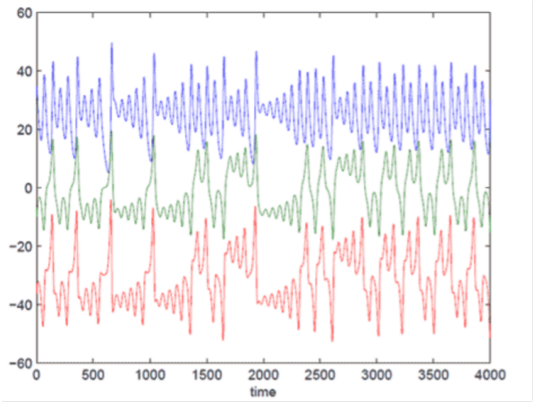

Figure 2: Time series for x (top), y (middle), z (bottom) variables, exhibiting chaotic solutions to Lorenz's equations for specific parameters. Data taken from [5].

It is also worth noting that all trajectories are confined in a fixed subspace of points in three dimensions. This boxed volume that each curve dances within is the strange attractor (simply because it doesn't trace a simple shape - it looks strange). And strangely enough, the attractor forms a double-lobed structure that resembles the wings of a butterfly - we commonly refer to this as the Lorenz attractor. The phenomenon of chaos is described by Lorenz himself as the "butterfly effect", depicting how small changes in input result in dramatically different outcomes in a complex system, akin to how the imperceptible flapping of a butterfly wings in Brazil could cause a tornado in Texas two weeks later [3].

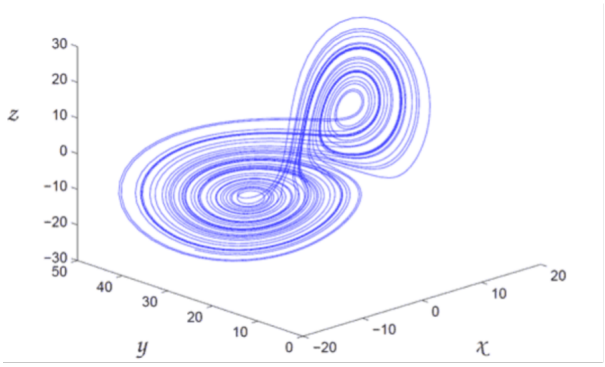

Figure 3: Three-dimensional phase space diagram of Lorenz's solutions. A phase space is an abstract space where each dimension represents a variable of the system, and a phase diagram helps visualise trajectories in the phase space by representing how the state of the system evolves over time. Diagram taken from [5].

In essence, chaos theory applies to any system whose behaviour appears random, unpredictable, and non-periodic, but is actually governed by deterministic laws. Since chaos is a feature of many physical models, it is intrinsically embedded in many natural systems, including the biological structure that enables our physical existence - the human heart.

The rate and rhythm of heartbeats are controlled by the cardiac conduction system and the autonomic nervous system (ANS) [6]. The conduction system is regulated by autorhythmic cardiac cells that generate electrical impulses without any external stimulation. Also known as pacemaker cells, they spontaneously dispatch electrical signals from the sinus node to depolarise and contract the atria (upper chambers of the heart). Following in Figure 4, the electrical signals then move down to the AV node, through the left and right branches of the bundle of His to finally arrive at the Purkinje fibres, whereby ventricular depolarisation and contraction follows. It is the coordinated contraction of the atria and ventricles that makes up a heartbeat [6].

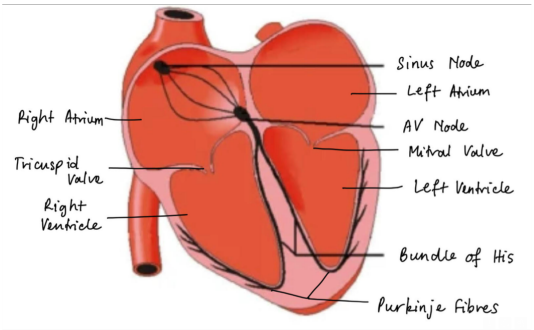

Figure 4: Labelled diagram of the heart. Diagram adapted from [7].

Thus, heart rate is indeed influenced by the pacing of spontaneous electrical activity from the sinus node. However, the pumping of blood throughout the body must also accommodate for stimuli such as changes in physical activity and emotional states. For this reason, the ANS - a component of the peripheral nervous system that regulates involuntary bodily functions, can also modulate the rhythm of pacemaker cells. Specifically, the sympathetic division of the ANS releases norepinephrine, a hormone and neurotransmitter that elevates heart rate during the body's 'fight or flight' response [6]. Conversely, the parasympathetic component of the ANS produces acetylcholine, a chemical signal that decreases heart rate to assist the body return to homeostasis after a period of stress [6].

In addition to the complex interplay between the involuntary nervous system and the spontaneity of autorhythmic cardiac cells, cells that make up the heart can also sense and respond to external forces. This mechanosensitive property means that the heart is regulated by mechanical as well as hormonal and electrical signals. Hence, it is very challenging to mathematically determine the conditions of the heart, making heart rate an output of what could be a chaotic system [6].

A 1991 study by Dr Ary L. Goldberg, a Harvard Professor of Medicine, explained that the most compelling clinical example of cardiac chaos is found in dynamics of a healthy heartrate, or the normal sinus rhythm [8]. This hypothesis is based on the observation that heart rate in healthy individuals is not strictly irregular, but displays self-similarity in its complex fluctuations at different orders of magnitude [8]. As shown in Figure 5, heartbeat can demonstrate the fractal nature of chaotic dynamics.

Furthermore, the normal (healthy) heart rate shows a phase

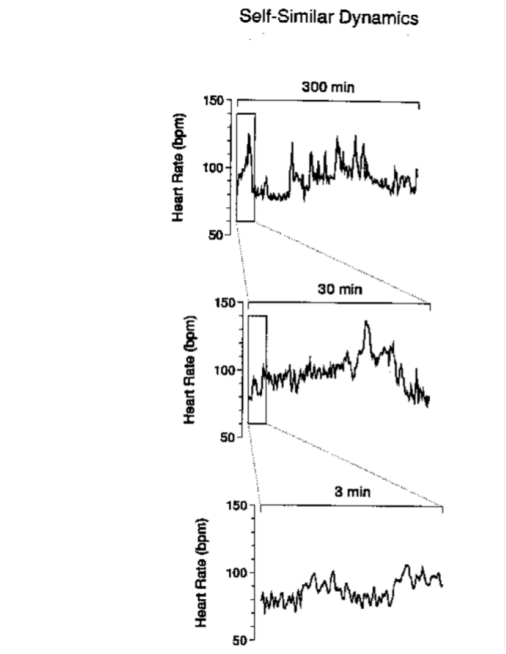

Figure 5: Time series of the normal sinus rhythm, displaying similar patterns in all time frames. Data taken from [8].

space plot consistent with an attractor. This is opposed to patients with pathological conditions, whose phase space plots depicts a structural collapse of the attractor. This is visualised in Figure 6 where the irregular trajectory was consistently associated with ventricular arrhythmia, a heart condition where autorhythmic cardiac cells in the ventricles (lower chambers of the heart) produce irregular electrical signals, resulting in an erratic rhythm of heart contractions.

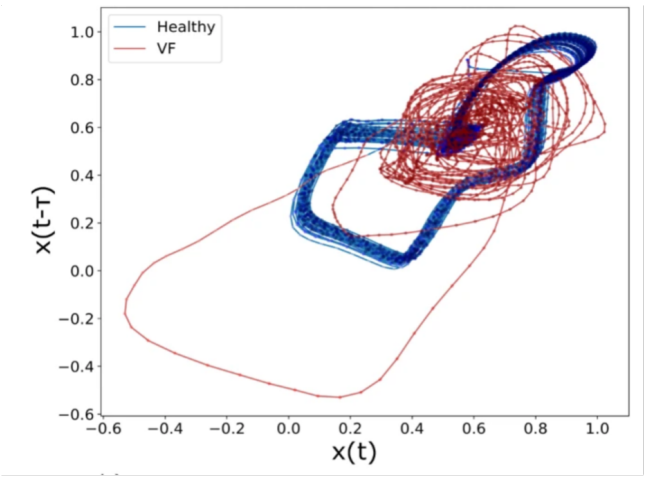

Figure 6: Phase space plots rendered from heart rate data of a healthy subject and a patient with ventricular fibrillation (VF). Graph taken from [9].

However, the question “Is normal heart rate chaotic?" has been widely discussed and examined, and most conclusions agree that the evidence was “inconclusive or negative" [10]. Arguments against Goldberg’s findings include discussions around whether chaotic dynamics of heart rate are purely ‘deterministic’ or part ‘stochastic’ (random) [11]. Various processes, such as the neurotransmitter release of acetylcholine by the ANS and the opening and closing of ion channels in pacemaker cells in the cardiac conduction system are understood to exhibit stochastic behaviours [10]. Even if the physiological mechanisms of cardiac activity are stochastic, deterministic equations have been shown to accurately approximate heartbeats [11]. This leads cardiologists to question how systems containing stochastic terms can be labelled as chaotic [10].

Leon Glass, a Professor of Physiology at McGill University who studied the application of nonlinear dynamics to cardiology, commented that the question “Is cardiac chaos normal or abnormal?" is futile unless it results in fresh insights on how heart rate can differentiate health and disease [9]. Instead, Glass suggests that the priority should be on understanding the patterns of complex cardiac patterns and their application to clinical settings [10].

Indeed, chaos analysis can be used to study attractors associated with specific heart diseases. This can be achieved by recording a single measurement in the cardiovascular system overtime, collecting, for example, the voltage of the ECG or the time series of a patient’s heart rate like shown in Figure 5. If the original time series is $x(t)$, it can be delayed to a later time $t+\tau$ to create a new variable $x(t+\tau)$ or $x(t-\tau)$, where τ is the time delay. When these variables are plotted against each other (Figure 6), the structure, or attractor, of the system emerges, allowing for its underlying complex dynamics to be reconstructed and studied [9].

Phase space diagrams reconstructed from time-delay systems can also present dimensions in place of variables. In Figure 7, E_1 is $x(t)$ and E_2 is $x(t+\tau)$ [13]. Through profound inspection of the abnormalities in ECG signals and their associated attractors, doctors may be able to recognise healthy trajectories and identify a large number of distinct heart diseases.

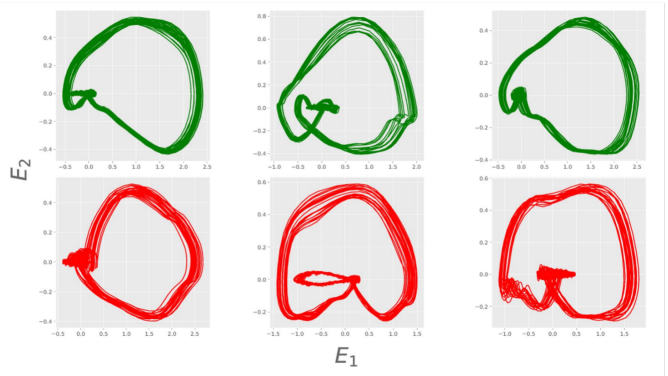

Figure 7: Two-dimensional projections of attractors for ECG signals of three healthy (top panel) and three unhealthy (bottom panel) cases. Diagram taken from [13].

In Lorenz’s own words, chaos occurs “when the present determines the future, but the approximate present does not approximately determine the future". By modelling cardiac data on phase diagrams and analysing the attractors shown, chaos theory has been proposed as an emerging tool for heart disease detection, perhaps enabling a more certain future for cardiac patients even as chaotic dynamics of the heart continue to be investigated.

Acknowledgement

I am grateful to Shelly Wickham for her review of an earlier draft of this article. Her perceptive feedback and thoughtful suggestions insightfully enhanced the discussions of both the physics and biological components.

Bibliography

[1] Gilmore C. Why is it so difficult to make a long-term weather forecast?. RTE; 2022 Aug 22.

[2] Becker E. Butterflies, rounding errors, and the chaos of climate models. NOAA Climate; 2017 Jul 27.

[3] Harvard University. Chaos Theory: A Brief Introduction IMHO.

[4] Xue B. The Lorenz System. Introduction to Biological Physics.

[5] Axelsen JB. Chaos theory and global warming: can climate be predicted?. Skeptical Science.

[6] Gordan R, Gwathmey JK, Xie LH. Autonomic and endocrine control of cardiovascular function. World J Cardiol 2015; 7(4): 204-214 [PMID: 25914789 DOI: 10.4330/wjc.v7.i4.204].

[7] Lima, G.S., Savi, M.A. & Bessa, W.M. Intelligent control of cardiac rhythms using artificial neural networks. Nonlinear Dyn 111, 11543-11557 (2023).

[8] Goldberger AL. Implications for Neuroautonomic Heart Rate Control in Health and Disease. Physionet.

[9] Tan, E., Algar, S.D., Corrêa, D. et al. Network representations of attractors for change point detection. Commun Phys 6, 340 (2023).

[10] Leon G. Introduction to Controversial Topics in Nonlinear Science: Is the Normal Heart Rate Chaotic?. Chaos 1 June 2009; 19 (2): 028501.

[11] Zhang JQ, Holden AV, Monfredi O, Boyett MR, Zhang H. Stochastic vagal modulation of cardiac pacemaking may lead to erroneous identification of cardiac "chaos". Chaos 1 June 2009; 19 (2): 028509.

[12] Gupter V, Mittal M, Mittal V. Chaos Theory: An Emerging Tool for Arrhythmia Detection. Sensing and Imaging 21(10) (2020).

[13] Shekatkar, S.M., Kotriwar, Y., Harikrishnan, K.P. et al. Detecting abnormality in heart dynamics from multifractal analysis of ECG signals. Sci Rep 7, 15127 (2017).

A Book Review on Inward Bound

By Shaun Parasher

There are many books that I would recommend to physicists or people who are simply curious about physics. Naturally, Leonard Susskind's books serve as a start for a gentle introduction to the foundations of modern physics. Feynman's lectures would be an excellent continuation from there. But, of course, physics isn't just about the equations, the experiments, and their interpretations. Physics has a rich and storied history, where the narrative behind famous theorems and discoveries are as exciting as their contents. To this end, the book I would recommend to anyone interested in the history of this sublime science would be Inward Bound by Abraham Pais.

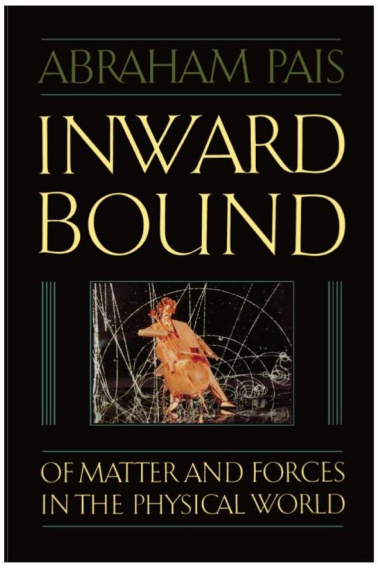

Figure 1: Oxford edition cover of Inward Bound. Image taken from [1].

Abraham Pais, a renowned Dutch physicist, is the perfect biographer to traverse the storied history of theoretical physics. Not only is he a maestro of the field (having worked in the prestigious Institute for Advanced Studies in Princeton), but he was a direct witting source to many of the key events and identities that shaped theoretical physics as we know it today. Many of his recounts begin with a personal anecdote shared with the titular physicist. Sometimes it will simply be a casual conversation with Niels Bohr over tea, and other times, intense rumination over quantum mechanical calculations alongside Feynman & Oppenheimer, et al. In either case, Pais imbibes his recounts with fond and fascinating passion.

Not only does Pais' personal proximity to seminal events in the history of theoretical physics give his prose a pleasant, organic comfort, but his fluent explanations of otherwise awfully sophisticated physics feels grounded and easy to pick up. Of course, Inward Bound is by no means a replacement for Matthew Schwartz's Quantum Field Theory, but Pais includes the relevant equations and explains their importance in the narrative of the development of quantum physics. The book's overarching narrative is made explicitly clear from the preface. Chapter 1 begins with Wilhelm Röntgen's discovery of X-Rays in 1895 and concludes with the discovery of the Z boson in the $U(1)$ experiment in 1983. Thus, the book's premise is to go from 'X to Z', presumably with the seventy-eight years of intermediate physics being 'Y'.

No detail is needlessly spared by Pais. After Röntgen's discovery comes the long exploration of cathode rays and the Geissler tube, culminating in J. J. Thomson's plum pudding model of the atom. The puzzles of radioactivity are steadily unveiled through Marie Curie's ascetic work. The true breakthrough is the UV catastrophe and Max Planck's spontaneous genius - the breakthroughs simply come tumbling out afterwards, and yet the timeline feels composed and well paced. Pais elegantly walks us through Ernest Rutherford's scattering experiment, upon which Niels Bohr develops his model of the atom. Fairly quickly we have arrived in the 1920s, and the dawn of quantum mechanics makes for the most exciting chapters as Dirac, Schrödinger, Heisenberg, and others develop the most remarkable (non-relativistic) theory of the atom. The question, however, of constructing a relativistic theory of light and matter interactions is saliently unanswered as we enter the war years.

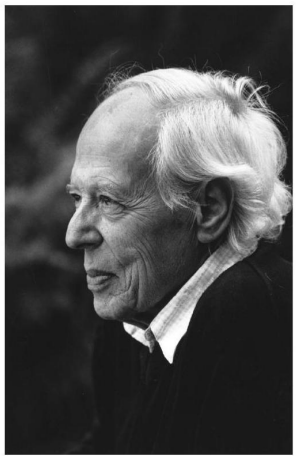

Figure 1: Abraham Pais by Joe Selsing. Image taken from [2].

Pais creates a page-turning tempo as he regales us with the frustrating infinities arising in perturbation theory and the need to unify special relativity and quantum mechanics. However, tensions arise not only in the physics. Being Jewish in the Netherlands during Hitler's occupation, Pais was forced into hiding before being briefly arrested at the end of the war. After some diplomatic quagmires, Pais was eventually able to emigrate to Princeton under Einstein's auspices. This shifting perspective illuminates the transition that theoretical physics underwent postwar; Europe's reputation as a bastion of theoretical physics and eminent thinkers began to tarnish, as Ernest Lawrence's 'big science' dogma flourished in America. The construction of particle accelerators such as the Bevatron, as well as large laboratories such as Lawrence Livermore and Los Alamos, meant that particle theories could be tested the same week they were concocted.

The Marquee event in postwar physics was the Shelter Island conference. Pais illuminates the significant intellectual fury stirred by the quest to unify relativity and quantum mechanics. It was Feynman, Schwinger and Tomonaga's work that eventually culminated in, arguably, one of science's best theoretical models: quantum electrodynamics. The theory was able to predict the anomalous magnetic moment of the electron to seven decimal places - an extraordinary feat! After the development of quantum electrodynamics, Pais reveals a deeper problem underlying particle physics - the particle zoo and the quest to develop gauge symmetries. Pais was deeply involved in these triumphs of mid-19th century physics, and provides a vaulting account of the unification of the electroweak force through quantum field theories, as well as the subsequent verification of the W and Z bosons during the $U(1)$ experiment. Admittedly, the equations and mathematical derivations presented in these chapters were most certainly above a level at which I could understand, but it was nevertheless intriguing to see these foreign equations reveal the deepest and most philosophically moving consequences for matter and fields. Pais' explanation of QFT is rewarding and his ambition to highlight the pinnacle of theoretical physics does not conflict with his ability to express the beauty in these complicated theories. It is this tour de force of engaging prose and exciting physics that makes this book a must read for physics enthusiasts.

The book ends on a tone of infectious optimism, with Pais expressing that there is still so much left unexplored in physics, musing "You ain't seen nothing yet". How exhilarating! Although Inward Bound can be somewhat hard to get your hands upon, it is certainly a must-read for anyone interested in physics. 9/10.

Bibliography

[1] Pais, A. (1986). Inward bound: of matter and forces in the physical world. Clarendon Press.

[2] Abraham Pais, ca. 1999. Photography by Joe Selsing.

Time, Trajectories and Chaos:
Simulating An N-Body System

By Maanya Sehjpal

"We see only snapshots, fixed forms, but nothing is static. We are immersed in a ceaseless becoming."

- Carlo Rovelli

The three-body problem - or more generally, the n-body problem - is known for its resistance to simple solutions. While Newton's laws provide a clean, solvable model for two interacting bodies, no general formula exists when a third is added.

With three or more masses, gravitational interactions become entangled. The system is still deterministic, but highly sensitive to initial conditions. Small differences grow exponentially over time, making long-term prediction nearly impossible. Seeing as natural celestial bodies tend to be influenced by more than one gravitational field, it is incredibly useful to have some method of predicting motion [1,3].

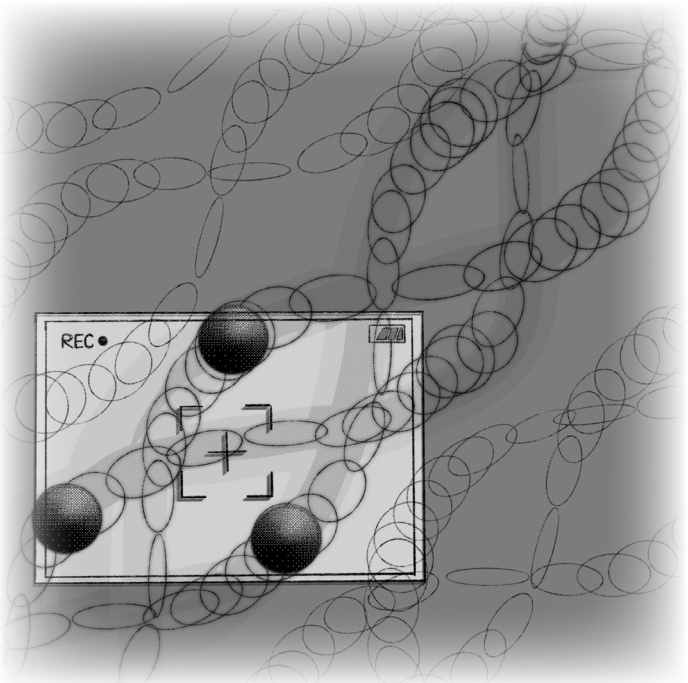

So, rather than solving the system, we simulate it.

A natural approach to tackling this problem is to create an algorithm that computes the gravitational forces acting upon each body at infinitesimal timesteps, and using that data to predict motion over a period of time. This can be achieved through simple Euler differentiation. However, as we quickly discovered, this leads to large margins of error when the solutions from this algorithm were compared with the known solutions for far simpler Simple Harmonic motion problems [3].

So instead, we turned instead to a more accurate method of prediction: Runge-Kutta four (RK4) differentiation. It looks at the current rate of change, estimates a midpoint, refines that guess, and then projects to the next full step.

Each of these guesses is weighted and combined into a single, more accurate update. Where Euler's method estimates the next state using a single slope (i.e., the derivative at the beginning of the interval), RK4 makes four calculations per time step:

1. $\mathbf{k}_1$ is the slope at the beginning of the interval.
2. $\mathbf{k}_2$ is the slope at the midpoint, using k_1 to estimate the value there.
3. $\mathbf{k}_3$ is another midpoint slope, using k_2 for its estimate.
4. $\mathbf{k}_4$ is the slope at the end of the interval, based on k_3.

In implementation, our RK4 loop calculates these values using functions for gravitational acceleration between bodies, storing intermediate "phantom" vectors for each body's guessed state at each sub-step. These phantom vectors are cleared and rebuilt at every iteration, ensuring that updates only occur after the full RK4 calculation is complete.

This method strikes a balance between computational speed and numerical accuracy, reducing cumulative error without significantly slowing the simulation (which is already a brute force algorithm). For a chaotic system like the n-body problem, RK4's stability is essential. [3]

We framed each body's state using phase space vectors - grouping position `x` and velocity `v` into a single vector '$\mathbf{y}$':

$$\mathbf{y} = [x, v]^\top \tag{1}$$

From Newton's second law, we know:

$$\frac{d\mathbf{y}}{dt} = [v, f(x)]^\top \tag{2}$$

where $f(x)$ is the gravitational acceleration on the body as a function of position. RK4 uses four progressively refined estimates (k_1 through k_4) to predict how $\mathbf{y}$ evolves over a small time step Δt.

$\mathbf{k_1}$ is the slope at the current time t_n:

$$\mathbf{k_1} = [v_n, f(x_n)]^\top \tag{3}$$

$\mathbf{k_2}$ samples the slope at the midpoint, using $\mathbf{k}_1$ to estimate the intermediate "phantom" state:

$$\mathbf{y}_{\text{intermediate}} = \mathbf{y}_n + \frac{\Delta t}{2} \cdot \mathbf{k}_1 = \begin{bmatrix} x_n + \frac{\Delta t}{2} \cdot v_n \\ v_n + \frac{\Delta t}{2} \cdot f(x_n) \end{bmatrix} \tag{4}$$

$$\mathbf{k}_2 = \begin{bmatrix} v_n + \frac{\Delta t}{2} \cdot f(x_n) \\ f\left(x_n + \frac{\Delta t}{2} \cdot v_n\right) \end{bmatrix} \tag{5}$$

$\mathbf{k_3}$ refines that midpoint using the result from $\mathbf{k_2}$:

$$\mathbf{k}_3 = \begin{bmatrix} v_n + \frac{\Delta t}{2} \cdot f\left(x_n + \frac{\Delta t}{2} \cdot v_n\right) \\ f\left(x_n + \frac{\Delta t}{2} \cdot \left(v_n + \frac{\Delta t}{2} \cdot f(x_n)\right)\right) \end{bmatrix} \tag{6}$$

$\mathbf{k_4}$ estimates the slope at the end of the interval:

$$\mathbf{k}_4 = \begin{bmatrix} v_n + \Delta t \cdot f\left(x_n + \frac{\Delta t}{2} \cdot \left(v_n + \frac{\Delta t}{2} \cdot f(x_n)\right)\right) \\ f\left(x_n + \Delta t \cdot \left(v_n + \frac{\Delta t}{2} \cdot f\left(x_n + \frac{\Delta t}{2} \cdot v_n\right)\right)\right) \end{bmatrix} \tag{7}$$

Finally, we update the full state vector with a weighted average:

$$\mathbf{y}_{n+1} = \mathbf{y}_n + \frac{\Delta t}{6}\left(\mathbf{k}_1 + 2\mathbf{k}_2 + 2\mathbf{k}_3 + \mathbf{k}_4\right) \tag{8}$$

This formulation lets us treat the system as a single evolving vector field, where each body's position and velocity are updated together in one sweep. One of the best design choices we made was to structure the simulation using phase space - that is, tracking both position and velocity together as a single state vector for each body.

This turns what could have been a tangle of separate variables into something clean and generalisable. It makes integration with RK4 easier, debugging simpler, and visualisation more intuitive. Instead of tracking dozens of separate values, each body has a single evolving footprint in phase space - a compact description of its past, present, and future motion.

Interestingly, when the same Simple Harmonic motion problems were run using the RK4 algorithm, the error was negligible. While it is not a perfect rendering of the n-body problem in a realistic sense, it allows us to have reasonable confidence in the simulation.

Building a Small Universe in Python

The following RK4 simulation was written in Python. Each celestial body was represented as a dictionary containing its mass, position, velocity, and a colour label for visualisation. These dictionaries were stored in a list - effectively a list of all active bodies in the system.

At each timestep, the program computed the total gravitational force on each body from all others. Intermediate estimates for velocity and position (used in RK4 integration) were calculated using temporary variables (- sometimes referred to in our notes as "phantom vectors"), which allowed all updates to be applied simultaneously after each full RK4 step.

By using phantom vectors, we ensured that intermediate RK4 steps didn't interfere with each other, thereby maintaining consistency and accuracy. All bodies were updated simultaneously after each full timestep.

Once the RK4 system was implemented, we tested it on various initial conditions from known mathematical solutions. Later, we created the visual rendering using Python's built-in libraries Matplotlib and FuncAnimation.

These outputs weren't just illustrations - they were phase portraits showing how the system evolved over time. All behaviour were deterministic, but extremely sensitive to the initial conditions. The code simply applied RK4 in a loop.

The core loop of the simulation proceeded in the following way:

1. For each body, calculate the total gravitational force from all other bodies using Newton's Law of Gravitation.

2. Apply the RK4 integration scheme using these accelerations, generating four intermediate vectors for each body.

3. Update each body's position and velocity only after the full RK4 step was completed ensuring consistency across bodies.

Once the core was working, we ran a series of simulations using carefully chosen initial conditions – some discovered from mathematical literature, others inspired by literature on periodic n-body orbits [2].

- The "Butterfly" shape (see Figure 1) emerged from a delicately tuned three-body configuration with near-mirror symmetry.

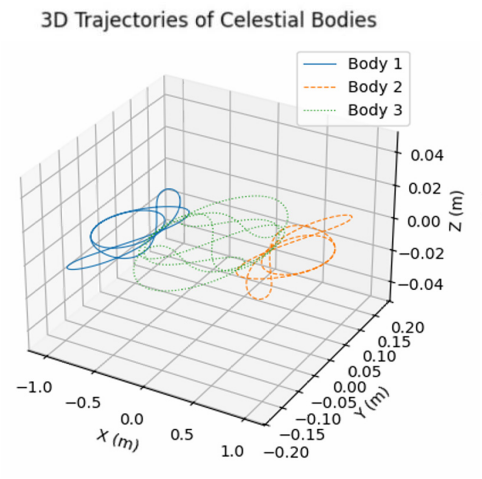

Figure 1: 'Butterfly'

- The "Figure Eight" orbit (Figure 2) is a rarely known solution to the three-body problem and was reconstructed using published coordinates.

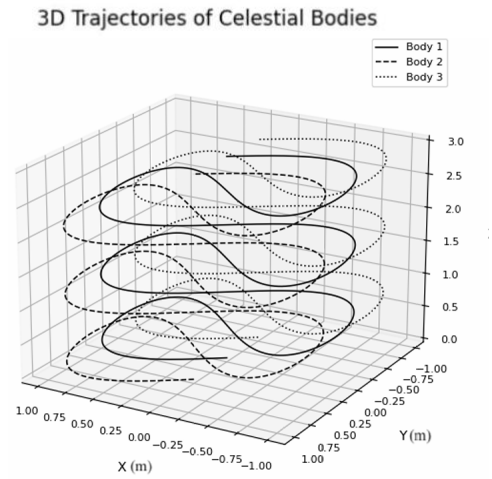

Figure 2: 'Ascending Figure Eight'

- The "Yin and Yang" path (Figure 3) came from an initial condition where two bodies began in mirrored orbits with just enough energy to trace one another's curves.

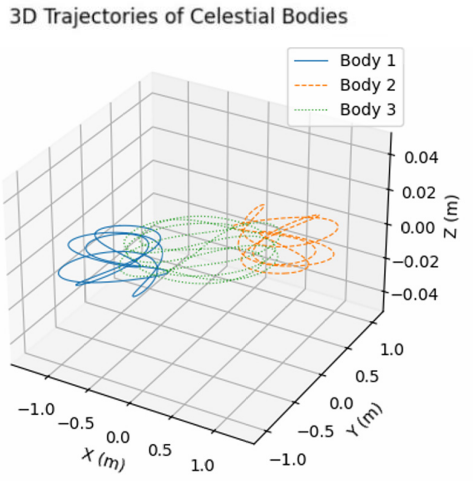

Figure 3: 'Yin and Yang'

Initial conditions for the 'Figure Eight' and related periodic orbits were sourced from solutions described in a Shanghai Jiaotong University paper [2]. These orbits, known as 'choreographies', exhibit striking symmetry.

These, however, are not just pretty visuals. They are dynamic signatures of deterministic chaos, drawn in real-time.

Even with RK4's relative accuracy, two simulations with slightly different inputs will eventually diverge. That's not a bug. That's the essence of chaos: sensitivity to initial conditions embedded in a deterministic framework.

Simulating chaos, then, isn't just about calculating positions. It's about recognising that in many-body problems, prediction has a horizon. You can simulate further – but the longer you go, the less reliable any precise outcome becomes.

What our simulation showed us wasn't control. It was sensitivity. Precision didn't give us certainty – it gave us an understanding of just how uncertain a deterministic system could be.

Credit for the core numerical implementation and RK4 integration goes to the very talented Charlie Abbey.

Bibliography

[1] Barrow-Green, J. (1997). Poincaré and the three body problem. Providence, RI: American Mathematical Society ; London.

[2] Li, X. and Liao, S. (2017). More than six hundred new families of Newtonian periodic planar collisionless three-body orbits. Science China Physics, Mechanics & Astronomy, 60(12). doi:https://doi.org/10.1007/s11433-017-9078-5.

[3] Musielak, Z.E. and Quarles, B. (2014). The three-body problem. Reports on Progress in Physics, 77(6), p.065901. doi:https://doi.org/10.1088/0034-4885/77/6/065901.

[4] NASA (2025). https://ssd.jpl.nasa.gov/ephem.html

A Cluttered Desk is a Cluttered Mind:

Neural Dynamics and Their Hallucinations as a Complex System

By Jude L. Metcalf

Physics and the Brain

The human brain is an incredible thing. Even the way a small part of the brain works to find the things we see every second is so rich, and gives us much to think about. There is some chaos to the dynamics of the brain in certain regimes, often as a result of the desire for pattern recognition being let loose and creating runaway feedback. It is *chaotic* in the technical sense that the brain functions as a very sensitive nonlinear system — but also *chaotic* in the normal sense. As we will see, the brain works with a lot of information at once, and somehow can still think straight. Most of the time.

Here we look at how modelling the primary visual cortex (V1) in two different ways will give chaotic responses, which each cause what we could call *hallucinations*; the self-driving responses of our neurons not connected to input vision. In the first case, we learn how the brain tries to recognise patterns and show them to us, hallucination-free. In the second part, we see how hallucinations become real in neuron dynamics.

V1, for our purposes, is a large network of around 140 million neurons, each of which is responsible for a single cell on the retina [1]. Neuroscientists are confident that V1 is responsible for very primitive image recognition, such as the response to contours, lines, shapes, and kinds of irritating irregularities in otherwise very neat and tidy patterns. Here we present one theory that V1 is part of a feedback loop with the rest of the brain, that tells you where interesting things are, and says *look over here! something interesting!* and you obey, and look. The technical term for a map of the interesting parts of an image is a **saliency map** — and so this theory is called the V1 Saliency Hypothesis or V1SH — pronounced *vish*.

The second model I present predicts the kinds of shapes and patterns we often see when coming in and out of anaesthesia, or under the effects of other substances, or just when we are very *very* tired. They are found to be the typically degenerate plane wave stable eigenfunctions of a Hamiltonian governing neuron dynamics in the brain. Physics methods come out of nowhere to show these patterns you could — theoretically — see yourself, with your very own eyes.

Where to Look, Where to See

Why is the way the brain sees the world and steers our eyes towards different places a good topic for a physics article? It may be argued that it is not. *But*, I think it is.

The problem of how to effectively construct a network (the brain) to make judgements upon huge amounts of data (visual objects), is a problem faced by physicists everywhere. The brain, or more specifically V1, shows time and again the elegant frameworks to judge significant amounts of data at once. And we don't need to go too far into the methods of modelling neurons to learn a lot.

V1SH and the Saliency Map

The best thoughts come from the most unexpected places, in physics and much else besides. We see some of the most important events coming from the everyday lives of the people who only later are given a voice in the world that couldn't accept them. For us, an idea came from an award-winning woman scientist who placed first in the competitive CUSPEA postgraduate examinations and would go on to found world-leading labs in renowned institutes of study. The story of Li Zhaoping and her 'V1 Saliency Hypothesis' is a testament to the strength and beauty of modern science.

What is V1SH? V1SH concerns V1 and its role in pre-processing the images presented to the eyes and sent through the brain. The hypothesis states that one of the roles of V1 is to create a map of visual input data and devote greater mental attention to certain areas of interest. This saliency map is made pre-attentively, before you can even think about it, to leave space for everything else our brain does. You wouldn't even recognise you're doing it, but every second we often make up to 3 of these gaze-fixing eye movements known as 'saccades' to the interesting parts of the world, often without realising it [4, 5]. V1SH gives a very concrete mathematical model of the map created by nonlinear neuronal dynamics which connect the individual correlations of neuron firing to the potential mapping activities of V1. And best of all, it has some quite good support from neuroscience which leads us to believe it's true!

The Model and the Math

The nonlinearity of the map from the intensity of light to saliency (1) will amplify certain objects in an image, and move the gaze to these more interesting features. A good model of our neurons requires both the excitatory neurons, as we model here, and "hidden" interneurons which interact between neurons to inhibit their interaction. This allows global oscillations of the saliency mapping strength about stable values [5]. We use the model which had been historically used before the model proposed by Zhaoping, but leads to large scale unstable hallucination [3].

While seemingly unwanted, the interneuron oscillations that are used in [5] stabilise vision and avoid global hallucinations. In other words, the oscillations don't allow V1 to settle into the kinds of hallucinations and chaotic instabilities of the kind we will see in the second part. Above are examples in Figures 0.1,0.2 of a particular instance of the model applied to a photo of a post, and to the Physoc logo.

I use the *bad*, chaotic, and hallucinatory map of intensity to saliency $\{I \to g(x)\}$ to demonstrate the V1SH features, with 'x' being the neuron potential. We use a differential equation of the neuron firing at every site 'i', as it interacts with all neurons 'j'. Importantly, the map $\{I \to g(x)\}$ is a stable fixed point of the differential equation at every neuron

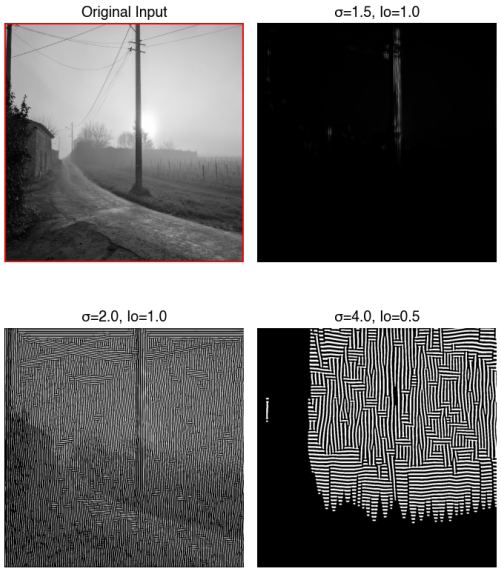

Figure 0.1: Along with Figure 0.2, here is a map $\{I \to g\}$ from our rudimentary V1SH model recognising verticality. The top left, red boxed image is the initial input which our V1 'sees', and the three other images are the outputs at different parameters. σ represents the strength of the vertical pattern recognition of the T matrix in (1), and Io is the I_o also in (1). Importantly, top right recognises well the verticality of the telephone pole, but much is to be desired in the byzantine patterns in the bottom.

Figure 0.2: The same model applied to the Physoc logo (see Figure 0.1). Again, the top right shows the verticality of certain letters well (especially 'H', 'Y', and 'O'), but hallucinates much in the bottom images.

with neuron potential. Even this simplified equation is quite ugly:

$$\dot{x}_i = -x_i + \sum_{\text{all } j} T_{i,j}\ g(x_j) + I_i + I_o \tag{1}$$

Let's unpack this, since it is not immediately obvious what this equation means. 'x', as we said, is the potential across the neuron, the only output that can be measured, or used in computation. The dynamics of the firing is controlled by the matrix of interactions between neurons i and j called T, with elements T_{ij}. The firing of neuron i is also controlled by the intensity of light seen by neuron i as I_i, and a nonlinear input I_o. I'll decompose these inputs in the following:

$$\boxed{\dot{x}_i = -x_i} + \sum_{\text{all } j} \boxed{T_{i,j}\ g(x_j)} + \boxed{I_i + I_o} \tag{2}$$

The solid box is very comfortable territory. This just tells us that the neuron firing is damped, and decays back to zero exponentially, all else being zero. On the other side, the dotted box can be seen as the neuron firing when the eye is exposed to some light I_i, along with a nonlinear feature of the neuron I_o which increases the firing rate to strongly pick out features of the intensity in an image.

The dashed box then holds the key information that we want. It links the neuron saliency across V1, allowing more global pattern recognition to attract gaze subconsciously with minimal devotion of brain power or attention. T will govern which patterns are picked out, for instance the symmetries of horizontal or vertical contours, length of contours, sizes of shapes, and so on.Then, the stable values of $g(x)$ will guide the eye to the interesting areas of the periphery.

We can see the hallucinations of our simple model in Figures 0.1,0.2. When the parameters are not quite right, the brain would make up patterns everywhere we look. Focus would be impossible, as our brain even creates patterns for itself, always on high-alert. Instead, brain dynamics are more complex than this simple model, and our job is to understand how the dynamics of long range interaction, time-dependence, and network features all act to stabilise V1 [5, 2].

Geometric Hallucinations

The previous part was focused on how the brain may be designed to intentionally pick out contours and shapes in the periphery to focus upon. This part shows how, given the right mental conditions, the unintentional dynamics of neuronal connections in V1 will cause the kind of hallucination characterised by a planewave with a wavelength of a characteristic structure in V1, the Hubel-Wiesel hypercolumn.

We will sadly not go so deeply into the mathematics of this case, which has been thoroughly examined elsewhere (in particular I take inspiration from [1]). All I want to present here is how the ideas, brought from physics make the analysis of these visual hallucinations clear and real. The Euclidean symmetry of the network of V1 neurons, their nonlinear interactions neurons, and runaway chaotic perturbations all combine to produce predictable dynamics. The strong eigenfunctions of these dynamics are the geometric hallucinations we notice in our vision (see Figure 0.4). It's been documented that, under the use of drugs, anaesthesia, or prolonged sleep deprivation, that such neuronal features will produce such conditions [1].

Neurons in V1 have been shown to have an orientation preference (see Figure 0.3), firing more often when presented with a contour at some angle $\phi \in [0, \pi]$. Experimentally, there are patches in V1 which contain all the orientation patches twice, such that travelling through the area, one can make a full 360° return to the original orientation. These patches have a characteristic area of around 2.67mm^2, with width of $1.33 - 2$mm (compare to the non-human patches of V1 in Figure 0.3). These excitingly named *Hubel-Wiesel hypercolumns* form units in a lattice of V1 containing in total approximately 1300 individual hypercolumns. Our modelling assumes this lattice to be almost continuous, with many lattice points, which opens much analysis of brain dynamics.

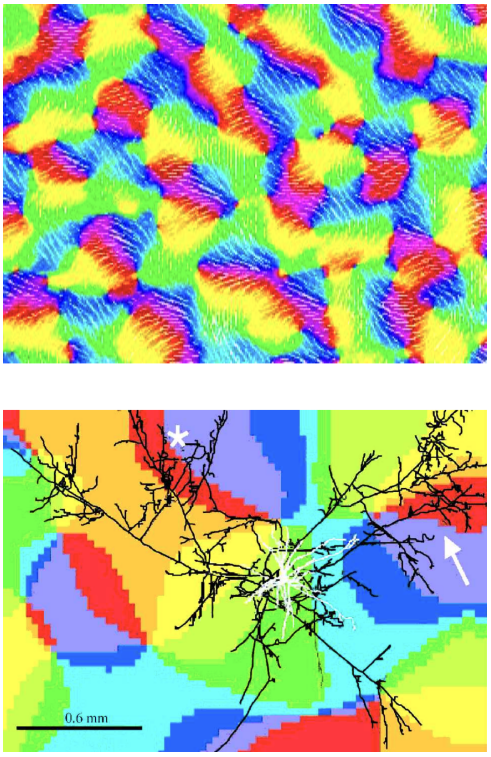

Figure 0.3: V1 of a macaque (top) and a cat (bottom), each with orientation preference mapped with their shade. The bottom cat V1 shows the long-range interneuron connections which in V1SH allow the oscillations which damp the hallucinations of pattern recognition, but in our current discussion can lead to a whole other order of hallucination. Image taken from [1].

Using very similar assumptions to those of the V1SH model in the first part, we divide V1 into hypercolumns, allowing excitation between neurons within each hypercolumn, and longer range inhibititory interactions between neurons in different hypercolumns, but only when they have the same orientation (see the interactions in the lower part of Figure 0.3). It's this combination of self excitation and long-range inhibition that produces a phase transition between good perception and geometric firing oscillations, seen as spirals, cobwebs, tunnels, and so on, when the neurons aquire certain firing properties.

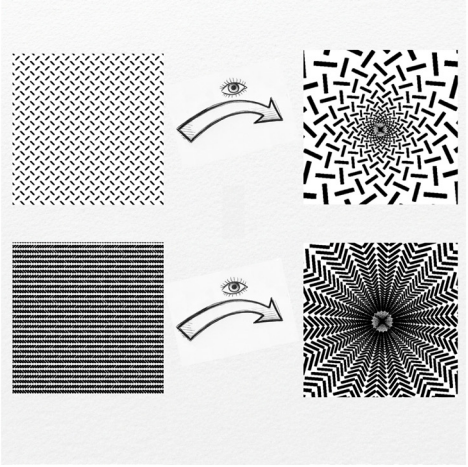

Figure 0.4: The mapping of 2D cartesian eigenfunctions of the symmetry transformations given from (3) to the polar coordinates of vision, as given in [1]. Here are just two of the eigenfunctions studied by them, and account for only one class of geometric hallucinations reported through time by many different people. I highly recommend the full analysis and explanation contained in the paper, from which these images were redrawn [1].

Equation (3) modelling the V1 neurons in their new regime is a continuous analogue to (1), since it assumes a very fine lattice of the hypercolumn domains in Figure 0.3. This model, as it concerns separate behaviour as well, is also a relabelling of functions from (1) to (3) as$\{x, g, T, I\} \to \{a, \sigma, w, h\}$. Furthermore, w is split into the short range hypercolumn self-interaction, and the long range intercolumn interactions. I will not explain this one, it can be an exercise for the reader bored enough to do so. . . :

$$\dot{a}(t) = -\alpha a(t) + \int_0^{\pi} \int_{\mathbb{R}^2} w(\mathbf{r}, \phi) \times \sigma[a(\mathbf{r}, \phi)] d\mathbf{r} d\phi + h(t) \quad (3)$$

Equation (3) above is a simplified version of (1) in [1]. When the big integral is small, we get the result that $a(t) = h(t)/\alpha$ is a stable solution. This has neurons seeing what is there, and reporting back to the brain, "*this spot is bright!*" or "*this spot is dim!*". However, when the neuron output function $\sigma[a(\mathbf{r}, \phi)]$ is steep, or if $w(\mathbf{r}, \phi)$ is strong enough, a will decouple with h. This creates oscillations in natural wavelengths of multiples of the width of a hypercolumn across V1 in complex patterns (see Figure 0.4). These conditions of strong, long range interactions and sensitive neuronal interaction have been shown to occur with hallucinogen usage, along with sleep deprivation, or with the administration of anaesthesia. The 2D eigenfunctions of the perturbation analysis and their corresponding polar hallucinations are given in Figure 0.4.

It's interesting that such physics methods and ideas of perturbation theory, spontaneous symmetry breaking, and bifurcations of nonlinear differential equations find such applications to the science of the brain, and give insight into the kinds of things we feel when not at our best.

Final Thoughts

The neuroscience of the small V1 — that makes up only about 0.1% of the neurons in our brain — is a strange inclusion into a physics magazine. But the topic of cognition, how we understand our own perception, and how we can understand how to use a lot of data at once, is exciting and important. Li Zhaoping points out that, per second, for every megabyte of information our eyes send to our brain, humans recognise only about 40 bits. That's like if you read a full book, and understood only a single word. In such a complex, interacting, strange network of buzzing neurons, it's incredible that we can see our friend in the corner of our eye, or remember a partner's face after many years, or even read any language *at all*.

The brain is the most worthy object of study, and physics is the best method of study (maybe). It's only natural that we understand more about ourselves, our intelligence, and what makes us happy by looking into the brain knowing all we know about science and the way the world works.

Bibliography

[1] Paul C. Bressloff, Jack D. Cowan, Martin Golubitsky, Peter J. Thomas, and Matthew C. Wiener. Geometric visual hallucinations, euclidean symmetry and the functional architecture of striate cortex. *Philosophical Transactions of the Royal Society of London. Series B: Biological Sciences*, 356(1407):299–330, 2001. doi: 10.1098/rstb.2000.0769.

[2] J.J. Hopfield. Neural networks and physical systems with emergent collective computational abilities. *Proceedings of the National Academy of Sciences*, 79(8):2554–2558, 1982.

[3] Zhaoping Li. Computational design and nonlinear dynamics of a recurrent network model of the primary visual cortex. *Neural Computation*, 13(8):1749–1780, 2001.

[4] Dale Purves, George J. Augustine, David Fitzpatrick, et al., editors. *Types of Eye Movements and Their Functions.* Sinauer Associates, Sunderland, MA, 2nd edition, 2001. URL `https://www.ncbi.nlm.nih.gov/books/NBK10991/`.

[5] Li Zhaoping. Vision: looking and seeing through our brain's information bottleneck, March 2025. arXiv:2503.18804 [q-bio].

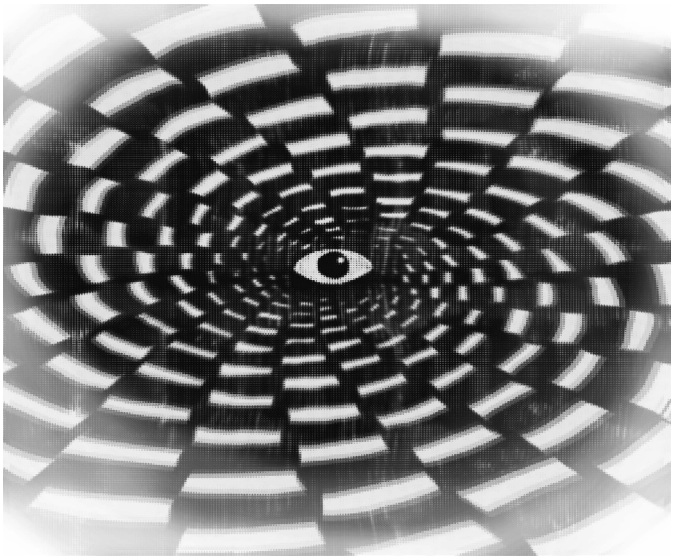

Cantor's Evil Function: When Intuition Fails

By Mani Shayestehfar and Thomas Zheng

To the naive mind of us undergraduate physicists, most functions we meet are friendly and kind; they are perfectly continuous, differentiable, and smooth enough to be Taylor-expanded when an approximation is needed. After all, *approximation* is one of physicists' greatest tools. These assumptions gradually become engraved into our minds. Maxwell's equations, Schrödinger's wavefunctions, and the simple harmonic oscillator, as well as many other well-known functions in physics, all behave nicely.

But this comfort is not universal. When we step into undergraduate mathematics courses, we are suddenly faced with formal and delicate proofs built on careful definitions, ε-δ arguments, and pathological examples that challenge our intuition. Physics students are often encouraged to focus on the core concepts and skip the details, with many mathematical proofs left as "exercises for the reader," in favour of physical insight. This difference in emphasis can lead us to overlook the delicate structure of the mathematics we rely on.

In this article, we explore an infamous example of a function which defies our intuition about what continuity and differentiability should look like: the *Cantor function*. To show that we should not brush aside these strange functions as mathematical oddities, we explore how this function appears in chaotic dynamical systems such as a pendulum driven by periodic force. But to explore these examples, we first need to introduce the notions of continuity and differentiability from a rigorous perspective, and that requires a precise definition of the notion of a limit, called the ε-δ defintion.

The ε-δ Definitions

The study of limits, infinite sums and calculus began in earnest in the 17th century with the work of Isaac Newton (1643–1727) and Gottfried Leibniz (1646–1716), and their work was followed by Leonhard Euler (1707–1783), the Bernoulli family (17th–18th century), and others. While these early mathematicians were able to produce many results, for example Euler's famous equality $\sum_{n=1}^{\infty} 1/n^2 = \pi^2/6$, they also encountered many paradoxes and contradictions when working with these infinite sums and limiting processes. In particular, the alternating harmonic series $\sum_{n=1}^{\infty}(-1)^{n+1}/n$ gave mathematicians a lot of grief: for details, Eddie Woo [2] has a nice video. It turns out that by rearranging the order in which you sum the terms $1, -\frac{1}{2}, \frac{1}{3}, -\frac{1}{4}, \frac{1}{5}, \ldots$ in the series, you can obtain any positive real number!

It wasn't until the 19th century when mathematicians began to develop the tools to resolve the paradoxes that arise when working with infinities. Their approach was to formalise the notions of limits, continuity and differentiability. In the book *The Paradoxes of the Infinite*, Bernard Bolzano (1781-1848) gave the modern definition of a limit, which states that the limit of a function $f(x)$ at $x = a$ is L, or $\lim_{x\to a} f(x) = L$, if

$$\begin{aligned}&\text{for each } \varepsilon > 0 \text{ there is a } \delta > 0\\ &\qquad\text{so that for all } x \text{ where } 0 < |x-a| < \delta,\\ &\qquad\qquad\text{we have } |f(x) - L| < \varepsilon\,. \quad (1)\end{aligned}$$

The best way to think of this definition is like a game. If your friend draws a vertical interval of width ε around the limit point L, the challenge for you is to find a horizontal interval of x-values around a so that the function f maps your interval inside of your friend's. Intuitively, we should be able to approximate L as closely as we want by taking x values sufficiently close to a.

Bolzano's work on limits was followed by Karl Weierstrass (1815-1897) who gave the modern definition of continuity, which states that $f(x)$ is continuous at $x = a$ if

$$\begin{aligned}&\text{for each } \varepsilon > 0 \text{ there is a } \delta > 0\\ &\qquad\text{so that for all } x \text{ where } |x-a| < \delta,\\ &\qquad\qquad\text{we have } |f(x) - f(a)| < \varepsilon \quad (2)\end{aligned}$$

The difference here is that a is contained within the domain of f where in the case of a limit, this might not be the case. Finally, the definition of a derivative is as follows: $f(x)$ is differentiable at $x = a$ if a is in the domain of f and there

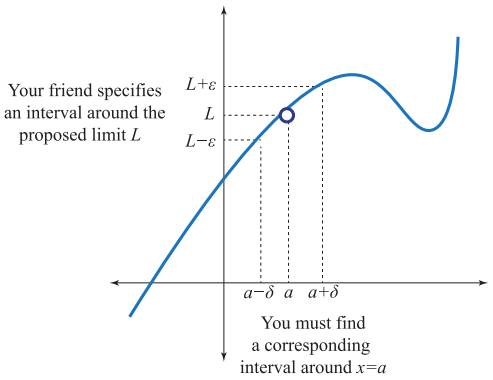

Figure 1: The $\varepsilon - \delta$ game.

exists the following familiar limit:

$$\lim_{x \to a} \frac{f(x) - f(a)}{x - a},$$

in which case we call the limiting value the derivative of $f(x)$ at $x = a$, written $f'(a)$. We can think of the derivative as the slope of $f(x)$ at the point $x = a$, where, in particular, constant functions that are flat have a derivative of zero.

An Unintuitive Function

It may be hard to imagine, but there exist functions that have a derivative of zero almost everywhere, yet increase monotonically from 0 to 1. One such example is the Cantor function $\mathrm{C} : [0,1] \to [0,1]$.

To explore this function, we first introduce the *Cantor set*. It is a closed subset of the interval $[0,1]$ and is defined recursively. Starting off with $[0,1]$, divide the interval into three equal sub-intervals of length $\frac{1}{3}$ each, and then cut out the open middle interval $\left(\frac{1}{3}, \frac{2}{3}\right)$. We define $\mathcal{C}_1 := \left[0, \frac{1}{3}\right] \cup \left[\frac{2}{3}, 1\right]$ to be the union of the remaining intervals. Then cut out the middle $\frac{1}{3^2}$ of the two closed intervals in $\mathcal{C}_1$ to get the four intervals $\mathcal{C}_2 := \left[0, \frac{1}{9}\right] \cup \left[\frac{2}{9}, \frac{1}{3}\right] \cup \left[\frac{2}{3}, \frac{7}{9}\right] \cup \left[\frac{8}{9}, 1\right]$. We can continue the process inductively – the limit of this process is defined to be the Cantor set, or $\mathcal{C} := \cap_{n=1}^{\infty} \mathcal{C}_n$.

Interestingly, if we keep track of how much we remove from $[0,1]$ each iteration, we obtain the geometric series

$$\frac{1}{3} + \frac{2}{3^2} + \frac{2^2}{3^3} + \cdots$$

which has a sum of one and hence the Cantor set $\mathcal{C}$ has zero length (or more formally, Lebesgue measure zero).

There is a wonderful interpretation of the numbers in the Cantor set. We are all familiar with the base 10 representation of a number $x \in [0,1]$, denoted $[x]_{10}$. Of course, we just write x in the usual way, i.e. $[x]_{10} = 0.x_1x_2\ldots$ where each digit x_j is in $\{0, 1 \ldots, 9\}$ and we interpret it as $x = \sum_{j=1}^{\infty} x_j/10^j$. However, we can also write x in its base 3, or *ternary, representation*

$$[x]_3 = 0.x_1x_2x_3\ldots \qquad \text{where each } x_j \in \{0,1,2\},$$
$$\text{and } x = \sum_{j=1}^{\infty} x_j/3^j\,. \tag{3}$$

The ternary representation $[x]_3$ provides us with geometric intuition for the values of the Cantor set. Recall that the first iteration $\mathcal{C}_1$ splits the interval $[0,1]$ into three equal sub-intervals. Notice that if $x_1 = 0$, then $x < 1/3$ so it falls in the first sub-interval. If $x_1 = 1$, then $x \in [\frac{1}{3}, \frac{2}{3})$ it falls in the middle sub-interval and if $x_1 = 2$, then $x \in [\frac{2}{3}, 1]$ so it falls into the last sub-interval. Similarly, x_2 represents the sub-interval that x belongs to in the next ternary subdivision. If we repeat this, we notice that the values of $x \in [0,1]$ that lie in the Cantor set are precisely those which do not have a 1 in their ternary representation.

We can now construct the Cantor function $\mathrm{C}(x)$ by defining the values of $\mathrm{C}(x)$ on the open intervals that we removed when constructing the Cantor set, and then extending $\mathrm{C}(x)$ to the entire interval $[0,1]$.

First, define the interval U_1 to be what we cut out of $[0,1]$ to get $\mathcal{C}_1$, i.e. $U_1 := [0,1] \setminus \mathcal{C}_1 = \left(\frac{1}{3}, \frac{2}{3}\right)$, and define $\mathrm{C}(x) = \frac{1}{2}$ for $x \in U_1$. Next, consider $U_2 := \left(\frac{1}{9}, \frac{2}{9}\right) \cup \left(\frac{7}{9}, \frac{8}{9}\right)$, which are the sub-intervals we cut out of $\mathcal{C}_1$ to get $\mathcal{C}_2$, or $U_2 := \mathcal{C}_1 \setminus \mathcal{C}_2$, and define $\mathrm{C}(x) = \frac{1}{4}$ for $x \in \left(\frac{1}{9}, \frac{2}{9}\right)$ and $\mathrm{C}(x) = \frac{3}{4}$ for $x \in \left(\frac{7}{9}, \frac{8}{9}\right)$. We can keep refining our definition inductively – for each n, define $U_n := \mathcal{C}_{n-1} \setminus \mathcal{C}_n$, which is the the union of 2^{n-1} open sub-intervals, and let C attain $1/2^n, 3/2^n, \cdots, (2^n - 1)/2^n$ on each sub-interval in order.

This defines C for all $x \in \cup_{n=1}^{\infty} U_n$, but we also need to define C for $x \in \mathcal{C}$. Since the points in the Cantor set are those without a 1 in their ternary expansion, we can simply define the Cantor function on these numbers to attain the value $\mathrm{C}(x) = \sum_{j=1}^{\infty} x_j/2^{j+1}$.

When we work through the definitions, it turns out that the Cantor function is continuous (the idea is that, as we continue refining the Cantor function to finer resolutions, the gaps between each horizontal step are filled in until we can move continuously). Moreover, the Cantor Function is constant and hence has a derivative of zero on each sub-interval, and we know that the sum of the lengths of these sub-intervals is one. Hence, for almost every value of $x \in [0,1]$, the Cantor function has derivative zero. Still, the Cantor function manages to creep up from 0 to 1! This may look like a wacky mathematical construction far removed from the physical world, but it appears in one of the simplest of physical systems...

A Chaotic Pendulum

You may ask: "OK. But surely the Cantor function belongs to the dark depths of pure mathematics". We ask you, our patient friend, to follow us in the following journey!

Let's look at the simple pendulum driven by a periodic force. [1]

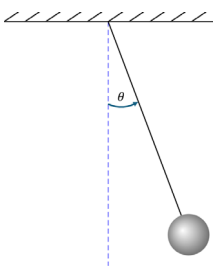

Figure 4: image of pendulum

The differential equation describing the change in the angle θ as a function of time t is

$$\alpha\ddot{\theta} + \beta\dot{\theta} + \gamma \sin\theta = A + B\cos(2\pi t), \tag{4}$$

[1] The following example is taken from Per Bak's *The Cantor function* [1].

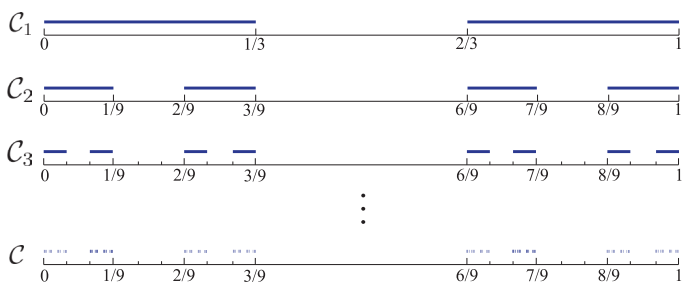

Figure 2: Construction of the Cantor set

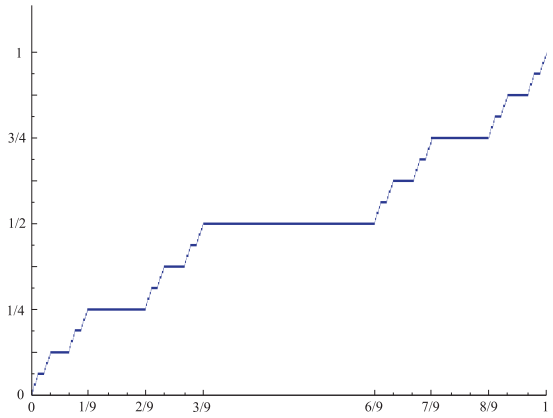

Figure 3: The Cantor Function is continuous and is constant on almost every $x \in [0, 1]$

where α is inertia, β is the damping, and γ is the gravitation constant. The periodic force component is given by the constant torque A and an external force with magnitude B which varies periodically due to the cosine term. Let us consider snapshots of this pendulum at discrete times $t = n$ where n is an integer, and so define the angle of the pendulum at time n, θ_n, alongside angular velocity, $\dot{\theta}_n$. Since equation (4) is a 2nd order ordinary differential equation, we can write the angle at $t = n + 1$, as a function P of $\theta_n and \dot{\theta}_n$,[2] i.e.

$$\theta_{n+1} = P(\theta_n, \dot{\theta}_n). \tag{5}$$

Due to damping, the long-term dynamics may settle onto a one dimensional attractor (a set to which the system evolves to). In this case, the angular velocity becomes a function of position: $\dot{\theta}_n = g(\theta_n)$, allowing the map P to be collapsed into one-dimension. Hence, we can write

$$\theta_{n+1} = P(\theta_n, g(\theta_n)) = f(\theta_n), \tag{6}$$

where f is a "circle" map, since it maps one point θ_n on the circle $0 < \theta < 2\pi$ onto another point θ_{n+1} on the circle. Even though equation (4) may not look too intimidating, the system is not always analytically solvable, and so we can expect to see periodic, quasi-periodic, and chaotic [3] solutions. There is nothing to fear, however. We can still study the qualitative behaviour of the system by considering a particular circle map f. The sine circle map is defined as

$$\theta_{n+1} = f(\theta_n) = \theta_n + \Omega + \frac{K}{2\pi} \sin(2\pi\theta_n), \tag{7}$$

where Ω is the bias term prescribing the frequency of the system in the case where the nonlinear coupling constant, K, is equal to 0. In studying this pendulum system, we are interested in observing how the pendulum locks in to a repeating pattern (i.e. studying its mode locking). Thus, we consider iterations of the sine circle map, $\theta_1, \theta_2, \theta_3, ...$ or, equivalently, $\theta, f(\theta), f^2(\theta), ...$ The long-term average angular displacement per iteration, or the *"winding number"* W, is defined as

$$W = \lim_{n\to\infty} \frac{f^n(\theta_1) - \theta_1}{n}. \tag{8}$$

[2]This construction defines a *Poincaré map*, which reduces the continuous-time dynamics of the pendulum to a discrete-time map by sampling the system once every drive cycle.

[3]Periodic motion repeats exactly after some number of steps, quasi-periodic motion never repeats but remains regular, and chaotic motion is irregular, highly sensitive to initial conditions, and non-repeating.

The winding number can obtain various forms depending on whether the system is periodic, quasi-periodic, or chaotic. For example, in the absence of nonlinear coupling (i.e. $K = 0$), $W = \Omega$. For small K, the system may exhibit periodic or quasi-periodic motion. If the trajectory is periodic, $W = p/q$ is rational, and if it is quasi-periodic, then W is irrational. When $K > 1$ (i.e. a high degree of nonlinearity), chaotic dynamics may emerge, in which case W can be highly sensitive to initial conditions and may fail to converge cleanly. Clearly Ω and K directly affect the winding number and hence the system's mode-locking (i.e. the system's tendency to settle into a repeating pattern with output frequency locked to a rational multiple of the input). *"Arnold's tongue"* highlights the regions in (Ω, K) plane where mode-locking occurs. Figure (5) shows these regions in the darker colour.

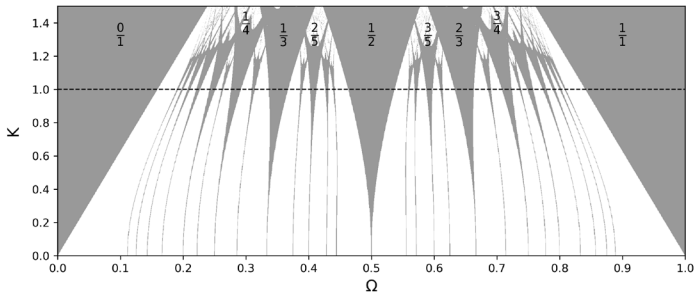

Figure 5: Arnold tongues of the sine circle map showing regions of mode-locking $W = p/q$ (darker colour) in the (Ω, K) plane. Tongues widen with higher K, and begin to overlap near $K \approx 1$, marking the onset of chaos.

For K close to zero, all mode-locking regions are quite small, so it is less likely that the winding number W is rational (it is more likely for it to be irrational), whereas for large K at the top, the regions of mode-locking widen in Ω, making rational winding numbers more common. This is reflected in the growing size of the Arnold tongues, visible in darker regions in figure (5).

Once we take a good look at this strange fractal, we may wonder if there is a $K > 1$ for which every Ω, rational or irrational, is part of the tongue, i.e. if every Ω is part of some mode-locked step when the system becomes highly nonlinear. If we consider various $\Delta(p/q)$'s, which is the size of the interval[4] in Ω over which the system locks into $W = p/q$, the

[4]can also be thought of as the horizontal width of the p/q tongue

plot of these intervals against W shows a staircase function with many similarities to the Cantor function in Figure 3 (Ω in horizontal, and W in vertical, axes). This function is continuous, non-decreasing, but constant (zero derivative) almost everywhere.

Including more steps results in a more filled-in Ω-axis and so to answer whether or not the mode-locked steps will eventually cover all of the Ω axis, we consider $S(r)$, the width of all steps wider than a given scale r. Indeed, the space between the steps, $1 - S(r)$, eventually shrinks to the Cantor set. In fact, empirically, the number of "holes" or "gaps" larger than the scale r, denoted $N(r)$, follows a power law: $N(r) \approx r^{-d}$. On a log-log plot, this appears as a straight line, consistent with fractal scaling. Power laws are especially interesting because they signal scale-invariant behaviour where the structure looks reasonably the same no matter how far you zoom in. This is a clear sign of fractals and critical phenomena in physics! To confirm this uncanny presence of the Cantor set, the exponent is $d \approx 0.87$, which is precisely the dimension of the Cantor set [5]. This result means that the space between the steps vanishes as r^{1-d} as $r \to 0$, implying that quasi-periodic motion occupies a set of measure zero, a fractal dust, and the system is mode-locked for almost all values of Ω.

In the end, what seems like a harmless, flat, staircase-shaped function turns out to mirror the hidden geometry of chaos. The Cantor function is not just a mathematical curiosity; it leaves its mark on real dynamical systems, reminding us that our intuition will almost certainly fail against rigour.

Bibliography

[1] Per Bak. The devil's staircase. *Physics Today*, 39(12): 38–45, 12 1986. ISSN 0031-9228. doi: 10.1063/1.881047. URL `https://doi.org/10.1063/1.881047`.

[2] Eddie Woo. The Mindblowing Alternating Harmonic Series. YouTube video, 2015. URL `https://www.youtube.com/watch?v=Q3nH02BsD-c`. Accessed on July 19, 2025.

[5] The fractal dimension quantifies how a set's detail or complexity scales with the size at which it is measured, often taking non-integer values.

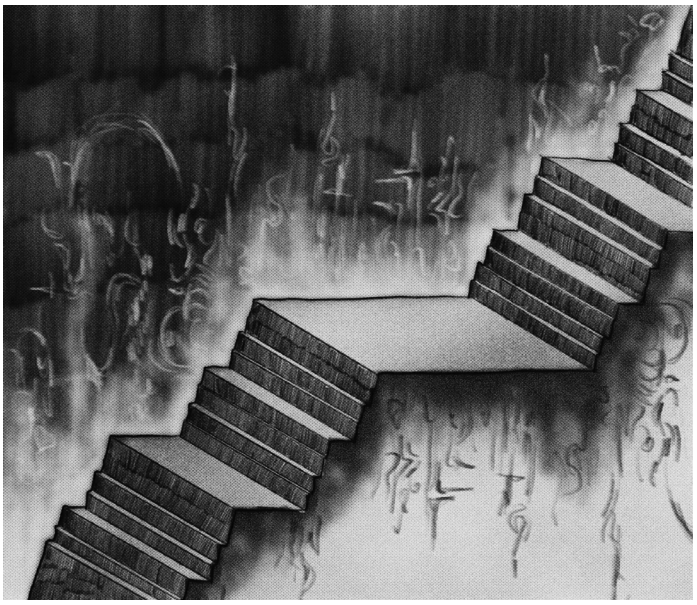

Spinors Part 1: Bloch Sphere and the Hopf Fibration

By Wayne Pooley and Richard Nicotra

1 Introduction

In introductory quantum mechanics, spin-$\frac{1}{2}$ systems are often given as the first example of a system where classical physics can't capture the full story. The Stern-Gerlach experiment, which involves shooting silver atoms through a magnetic field and measuring their deflection, defies classical intuition – we observe only a discrete spectrum of magnetic moments (and hence angular momenta), as opposed to a continuous range of values. This led to the development of quantised theories of angular momentum and the description of an additional intrinsic quantum property, called spin. For the electrons in the silver atoms, which are spin-$\frac{1}{2}$ particles, they can take a binary spectrum: spin up and spin down.

When measured, the spins of particles like electrons behave probabilistically. The state of the electron before measurement is described by an expression called the *wave function*, denoted $|\psi\rangle$. In the Stern-Gerlach experiment, the particle's interaction with the magnetic field and subsequent measurement method alters this wave function. Due to the probabilistic nature of the wave function, we can only know the probabilities of the associated pure states (spin up or down). Furthermore, measuring a mutually orthogonal spin axis after the initial measurement erases the information encoded in the original state, meaning the wave function describing the original spin axis returns to being a superposition of states rather than a pure state.

This is where most of us come across the Bloch sphere as a way to represent these qubit systems (qubit being short for quantum bit, since it can be in any superposition of the two pure states). The Bloch sphere is an informative visual tool that represents the space of states for our qubit's wave function and how it can evolve with time. However, many of its mathematical underpinnings are left to students to study individually; in aid of this pursuit, we aim to explain more of the mathematical background that underlies this modest ball and the wider theory of spinors in a series of two articles, of which this is the first (Part 2 will be published in the next Jeremy issue).

2 The full story made short

Here is our journey for Part 1 laid out from start to finish:

$$\begin{array}{ccc} & & \mathbb{C}^2 \\ & & \uparrow \\ S^3 & \longrightarrow & S^2 \cong \mathbb{CP}^1 \end{array}$$

where the hook-arrow denotes an *embedding* of one space into another. We will explain and motivate each step along these

paths as we go along.

3 The short story made long

Our qubit's wave function, denoted $|\psi\rangle$, can be influenced and interfered with by the system in ways reminiscent of physical waves. This motivates the use of complex numbers in the construction of our state space. We treat the two independent measurement outcomes (spin up and down) as two linearly independent vectors $|+\rangle$ and $|-\rangle$ respectively, and then allow these vectors to be scaled by complex coefficients α, β. Thus, our state space is $\mathbb{C}^2$.

Motivated by the idea that measuring the "overlap" of states can predict the probability of transitioning from one state to another, we introduce an inner product on our finite-dimensional vector space, given by

$$\langle\psi|\varphi\rangle = \alpha_\psi^* \alpha_\varphi + \beta_\psi^* \beta_\varphi. \tag{1}$$

where $*$ denotes complex conjugation. This leads to the notion of a norm on our state space given by [1]

$$||\,|\psi\rangle\,|| = \sqrt{\langle\psi|\psi\rangle} = \sqrt{|\alpha|^2 + |\beta|^2}, \tag{2}$$

to ensure our probabilities add up to 1, our state vectors are normalised such that $|\alpha|^2 + |\beta|^2 = 1$. With these features of the inner product and *completeness* (where Cauchy sequences converge from a finite-dimensional vector space), we get a *Hilbert space*, which is the typical type of space needed for representing a quantum system.

The normalisation of $\mathbb{C}^2$ vectors maps states $|\psi\rangle \mapsto \frac{|\psi\rangle}{||\,|\psi\rangle\,||}$, meaning states that differ only by a multiple of a real number are mapped to the same unit vector, called a *spinor*. These live on the unit 3-sphere

$$S^3 = \{(x, y, z) : x^2 + y^2 + z^2 = 1\} \tag{3}$$

which is described by three real coordinates embedded in a two complex-dimensional (i.e. four real-dimensional) space. Hence, we write $S^3 \hookrightarrow \mathbb{C}^2$. However, there is another form of redundancy in our states. Any two states that differ by a multiple of a global phase $e^{i\theta}$ are indistinguishable by measurements according to the Born rule, so they represent the same physical state despite being different spinors. Thus, the physical state space can be thought of as the set of "equivalence classes" of spinors when we divide out a factor of $e^{i\theta}$. This is what we call the Bloch sphere.

4 First Group Connections

We begin by outlining the relevant groups needed to discuss the formalism behind the Bloch sphere's construction.

The unitary group of degree one

$$\mathrm{U}(1) = \{z \in \mathbb{C} : |z| = 1\} \tag{4}$$

is the set of complex numbers with magnitude 1. These are of the form $e^{i\theta}$, where θ is some angle. Thus, U(1) is simply the unit circle in $\mathbb{C}$ and its topology is identified with the circle S^1.

[1] This is just the discrete L^2-norm.

The Special Unitary group of degree 2

$$\mathrm{SU}(2) = \{U \in \mathrm{Mat}_{2\times 2}(\mathbb{C}) : U^\dagger U = I, \det U = 1\} \tag{5}$$

has elements of the form

$$U = \begin{pmatrix} \alpha & -\beta^* \\ \beta & \alpha^* \end{pmatrix}. \tag{6}$$

The determinant condition is equivalent to

$$|\alpha|^2 + |\beta|^2 = 1, \tag{7}$$

which should ring some bells – this is the norm-squared of a spinor $|\psi\rangle = [\alpha, \beta] \in S^3 \hookrightarrow \mathbb{C}^2$. SU(2) is also described with 3 real components (like spinors prior to the removal of global phase), so one can construct a *diffeomorphism* from $\mathrm{SU}(2) \to S^3$ that allows us to identify the group SU(2) with the topological structure of S^3 and vice versa:

$$[\alpha, \beta] \mapsto U = \begin{pmatrix} \alpha & -\beta^* \\ \beta & \alpha^* \end{pmatrix} \in \mathrm{SU}(2)$$

Therefore, the 3-sphere $S^3 \cong \mathrm{SU}(2)$ as smooth manifolds, and we find that spinors and their corresponding SU(2) matrices encode the same information. The matrix contains the corresponding spinor as its first column and its orthonormal pair as the second column, satisfying the $\det U = 1$ condition. However, there is a difference between a SU(2) matrix and its corresponding spinor, and that difference is that the former can act on the latter to transform spin states; this difference, and its consequences, will be made clear in the mathematical formalism developed in Part 2 of this series.

5 Spinors and the Riemann Sphere

We're now going to slow down and consider spinors from first principles, along the way discussing how:

1. Spinors represent a body's rotation by encoding information about the axis and direction of rotation.

2. Spinors that are orthogonal represent antipodal states on the Bloch sphere, and vice versa. (This seems unintuitive because orthogonal vectors are usually thought of as being perpendicular, not opposite.)

3. Rotating the physical state space by an angle 2π returns the spinor $-|\psi\rangle$, and rotating again by 2π gets you back to $|\psi\rangle$. In general, rotating a physical state vector by a given angle only rotates the corresponding spinor by half that angle, and vice versa.

In fact, only the first two properties will be discussed here. The third will be thoroughly discussed in Part 2 of this series.

Although the Bloch sphere provides a way of visualising the physical states, it doesn't immediately help to visualise transformations. Meanwhile, spinors often seem unintuitive because there isn't an easy way to plot them or their transformations, since we need four dimensions to plot S^3 and visualise the effect of multiplying a spinor by an SU(2) matrix. Instead, we look at the construction of spinors and their transformations through the lens of the Riemann sphere.The Riemann sphere is the most

basic object in complex analysis as it provides the codomain for general complex functions. A thorough and simultaneously approachable treatment can be found in [2]. We will show that it coincides with the Bloch sphere through its shared equivalence to the complex projective line $\mathbb{CP}^1$, and construct the theory of spinors around it. In Part 2, we will see that the additional complex structure it wields allows for a better (and animatable) visualisation of spinor transformations.

The Riemann sphere is $\mathbb{CP}^1$ is the Bloch sphere

We begin by showing how to construct the Riemann sphere using stereographic projection. Let us start with the unit sphere S^2 embedded in $\mathbb{R}^3$ and centred on the origin. Then, overlay the complex plane $\mathbb{C}^1$ onto the xy plane such that the real axis overlaps the x-axis and the imaginary axis the y-axis. Then for any point (x, y, z) on S^2, its stereographic projection is the complex number ζ that sits at the intersection of the xy plane and the line connecting the South Pole to (x, y, z). (See Fig. 1.) Algebraically, this defines the map

$$(x, y, z) \mapsto \frac{x + iy}{1 + z}, \tag{8}$$

which has the inverse

$$\zeta \mapsto \left(\frac{2\mathrm{Re}(\zeta)}{1 + \zeta\zeta^*}, \frac{2\mathrm{Im}(\zeta)}{1 + \zeta\zeta^*}, \frac{1 - \zeta\zeta^*}{1 + \zeta\zeta^*} \right). \tag{9}$$

The North Pole is mapped to 0, the equator $x^2 + y^2 = 1$ is mapped to the unit circle $S^1 \equiv \mathrm{U}(1)$, and the entire northern hemisphere is mapped to the interior of the unit disc. Similarly, the southern hemisphere is mapped to the exterior (i.e. complement) of the unit disc. However, as the point on the sphere approaches the South Pole, the projection line approaches horizontal and the modulus of the projected number grows without bound; hence we introduce a "number at infinity", called ∞, and set the projection of the South Pole to be this point. The resulting set

$$\overline{\mathbb{C}} := \mathbb{C} \cup \{\infty\} \tag{10}$$

is called the extended complex plane, and the stereographic projection is a homeomorphism between it and the sphere, thus allowing us to treat the two objects as topologically equivalent and justifying the name "Riemann sphere".

The complex projective line $\mathbb{CP}^1$ is constructed by starting with $\mathbb{C}^2 \setminus [0, 0]$ and quotienting out the equivalence relation $[a, b] \sim \lambda[a, b] \quad \forall \lambda \in \mathbb{C} \setminus \{0\}$, so that all scalar multiples of vectors are made equivalent. Denoting the equivalence class of $[a, b]$ as $[a : b]$, the easiest choice of representative when $b \neq 0$ is $[a/b, 1]$, while for $b = 0$ there is only one equivalence class $[1 : 0]$. Thus, the complex projective line is

$$\mathbb{CP}^1 = \{[\zeta : 1] : \zeta \in \mathbb{C}\} \cup \{[1 : 0]\}, \tag{11}$$

and we can see by comparison with Eq. (10) that the set on the left is isomorphic to $\mathbb{C}$ while $[1 : 0]$ is equivalent to the point at infinity, thus demonstrating its correspondence to $\overline{\mathbb{C}}$ as constructed above. Notice what we have done here is construct the Bloch sphere in one step: when we constructed it in Section 3, we normalised our $\mathbb{C}^2$ vectors first (quotienting out the real modulus), and afterwards quotiented out the global phases $e^{i\theta}$, meaning that in total we quotiented out multiplication by a complex number in modulus-argument form. This is exactly what we have done here, demonstrating the equivalence of $\mathbb{CP}^1$ and the Bloch sphere. Since we have also shown equivalence to the Riemann sphere, which is topologically equivalent to S^2, we have shown that $S^2 \cong \mathbb{CP}^1$ as stated in Section 2.

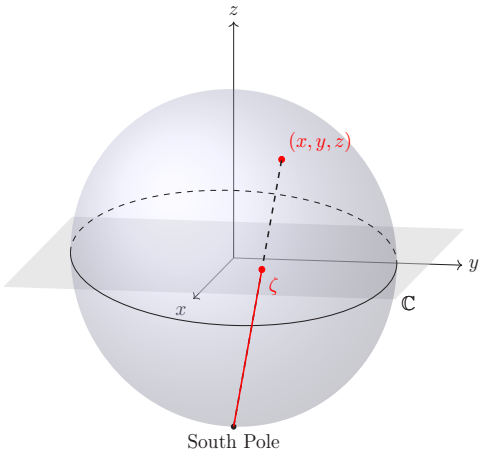

Figure 1: Stereographic Projection of the point (x, y, z) on the unit sphere to $\zeta \in \mathbb{C}$.

Spinors according to Riemann (sphere)

Now, equipped with the Riemann sphere and its connection with $\mathbb{CP}^1$ and the Bloch sphere, we are ready to discuss how to represent rotation axis and direction using spinors. Let

$$\chi \in \mathbb{C}^2, \quad \chi = [\chi_1, \chi_2] \tag{12}$$

denote what will become a spinor, and since this will represent a quantum state, assume it is normalised such that $|\chi_1|^2 + |\chi_2|^2 = 1$. (Normally, we would use column vectors here, but we'll stick to row vectors for now.) For a vector $(x, y, z) \in S^2$, we can use Eq. (8) to get the corresponding point on the Riemann sphere:

$$(x, y, z) \mapsto \frac{x + iy}{1 + z} = \zeta, \tag{13}$$

which we can suggestively write as the ratio of two complex numbers

$$\zeta = \frac{\chi_1}{\chi_2}, \quad \chi_1 = \alpha(x + iy), \quad \chi_2 = \alpha(1 + z). \tag{14}$$

where $\alpha \in \mathbb{C}$ is a normalisation constant. It turns out that

$$[\chi_1, \chi_2] = [\alpha(x + iy), \alpha(1 + z)] \tag{15}$$

is a spinor representation of (x, y, z) [1], and we can use the normalisation requirement to show that

$$|\alpha| = \frac{1}{\sqrt{2(1 + z)}}. \tag{16}$$

However, $\theta := \arg \alpha$ is a free parameter in this representation, so there is an infinite family of spinors that represent this S^2 vector, given by the general spinor representation

$$\chi = \left[\frac{x + iy}{\sqrt{2(1 + z)}} e^{i\theta}, \sqrt{\frac{1 + z}{2}} e^{i\theta} \right] .I \tag{17}$$

This form can be immediately connected to the Bloch sphere, as the immeasurable $e^{i\theta}$ global phase has been extracted from the rest of the expression. Thus we can quotient it out to get the physical state

$$\chi \sim \left[\frac{x+iy}{\sqrt{2(1+z)}}, \sqrt{\frac{1+z}{2}}\right]. \tag{18}$$

This is a basic realisation of the map $S^3 \to S^2$ referenced in Section 2, called the Hopf fibration, which we will discuss more abstractly (and more generally) in Section 6.

Now, if we are given a spinor $[\chi_1, \chi_2]$ with $\chi_2 \neq 0$, we can always divide by χ_2 to get

$$\chi \sim \left[\frac{x+iy}{1+z}, 1\right] \in \left[\frac{x+iy}{1+z} : 1\right] \sim \frac{x+iy}{1+z} \in \overline{\mathbb{C}}, \tag{19}$$

Such a spinor can always be associated with a unique equivalence class $[\zeta : 1] \in \mathbb{CP}^1$, and hence with a unique complex number ζ on the Riemann sphere. Similarly, when $\chi_2 = 0$, the corresponding equivalence class is $[1 : 0]$, and hence the corresponding point on the Riemann sphere is ∞. This is the mathematical realisation of the equivalence of the Bloch sphere, Riemann sphere, and $\mathbb{CP}^1$.

So up to global phase, spinors are just equivalent to numbers on the Riemann sphere! This seems to be making things more complicated for no reason, but as we'll see here and in Part 2, it's a very powerful change in perspective, as the properties of spinors we listed at the beginning of Section 5 become much easier to show and visualise.

Spinors, Orthogonality, and Antipodal States

First, while every vector $(x, y, z) \in S^2$ has a U(1) family of non-identical spinors representing it, a given spinor always uniquely determines the vector (x, y, z) it represents, which can be found by first converting it to the equivalent complex number and then using the inverse stereographic projection.

Second, antipodal vectors in S^2 have orthogonal spinor representations, and vice versa. The forward implication is just a simple calculation: use Eq. (8) to get the spinor representations of (x, y, z) and $(-x, -y, -z)$ and take their inner product, simplifying using the fact that $x^2 + y^2 + z^2 = 1$ to show that it is zero. In fact, we can replace the spinor representations of (x, y, z) and $(-x, -y, -z)$ with any elements of the corresponding $\mathbb{CP}^1$ equivalence classes and still get an inner product of 0, confirming that the spinor representations for opposite physical spin states never overlap, regardless of phase. The reverse implication requires showing orthogonal spinors always represent antipodal vectors, and this can be shown using a combination of algebraic and geometric arguments, as follows.

Suppose $[a, b]$ and $[c, d]$ are orthogonal spinors, and further suppose we have eliminated the global phase so that b and d are both real. Then (recalling $*$ denotes complex conjugation), orthogonality gives us

$$ac^* + bd = 0 \iff \frac{|a|}{b} e^{i \arg(a)} = \frac{d}{|c|} e^{i(\arg(c) - \pi)}, \tag{20}$$

which can only be satisfied without breaking the normalisation of the spinors if

$$d = |a|, |c| = b, \arg(c) = \arg(a) + \pi. \tag{21}$$

Thus, we must have

$$[c, d] = \left[be^{i(\arg(a)+\pi)}, |a|\right], \tag{22}$$

Exploiting the fact that orthogonality is independent of the choice of representatives, we can divide by $e^{i(\arg(a)+\pi)}$ to choose the more interpretable representative

$$[c, d] \sim \left[b, |a|e^{i(\arg(a)+\pi)}\right] = [b^*, -a^*], \tag{23}$$

where we have used that b is real so that $b = b^*$. Clearly, the inner product of $[a, b]$ and $[b^*, -a^*]$ is still zero as we expect, but now the corresponding Riemann sphere equivalents of the physical states are

$$[a, b] \sim \left[\frac{a}{b} : 1\right] \sim \frac{a}{b} \in \overline{\mathbb{C}} \tag{24}$$

and

$$[b^*, -a^*] \sim \left[-\frac{b^*}{a^*} : 1\right] \sim -\frac{b^*}{a^*} = -\left(\left(\frac{a}{b}\right)^{-1}\right)^* \in \overline{\mathbb{C}}. \tag{25}$$

This latter number is just $\frac{a}{b}$ after undergoing inversion, complex conjugation, and multiplication by -1, the composition of which can be easily interpreted geometrically in polar coordinates:

$$\frac{a}{b} = re^{i\theta} \mapsto \frac{1}{r}e^{-i\theta} \mapsto \frac{1}{r}e^{i\theta} \mapsto \frac{1}{r}e^{i(\theta+\pi)} \tag{26}$$

So this process rotates $\frac{a}{b}$ a half turn about 0 and inverts its modulus. When viewed through the lens of the inverse stereographic projection, it is exactly the process that sends a number on the Riemann sphere to its antipodal point! More loosely, since the quotienting process makes points separated by a half turn about the origin (like $[x, y]$ and $[-x, -y]$) equivalent, half turns in $\mathbb{C}^2$ become full turns in $\mathbb{CP}^1$, and quarter turns become half turns. The seemingly strange tendency for orthogonal spinors to correspond to antipodal states makes perfect sense.

6 Bundles

Equipped with our mathematical understanding of spinors and orthogonality, we are now in a position to understand the most general construction of the mapping from spinors to physical states, using bundles and the Hopf fibration.

Let E, B, and F be topological spaces. E is our *total space*, which can be thought of as the big space that we want to map to the "smaller" *base space* of the bundle B. In some small neighbourhood of our total space, it is said to "look like" the *product space* $B \times F$; more precisely, there is a homeomorphism φ from $V \subset E$ to a local neighbourhood $W \subset B \times F$. This is called *local triviality*. The total space does not necessarily have the same global topology as the product space, which is what makes the mapping π (the projection of the bundle) from the total space to the base space unique. Furthermore, there exists a map proj_1 (projection to the first factor), that takes us from the product space $B \times F$ to the base space B, forming the commutative diagram:

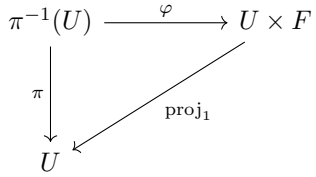

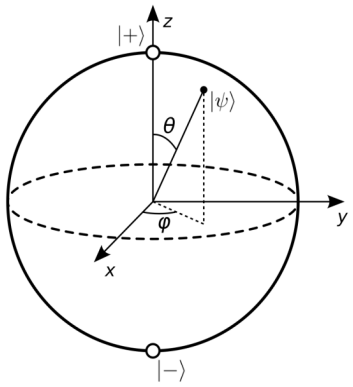

Figure 2: Bloch sphere with (orthogonal) spin up and spin down states marked at antipodal points. [4]

where $U \subset B$ is a subset of the base space, $U \times F$ is a subset of the product space, and $\pi^{-1}(U) \subset E$ is a subset of the total space. The specific case where the total space and product space coincide is called the trivial fibre bundle, and the projection of the fibre π is just the projection onto the first factor.

Hopf Fibration

We finally reach the meat and potatoes of the matter. This is what all the set-up and construction have been marching towards – our friendly Bloch sphere visualisation! We pick up the story here with spinors S^3 in $\mathbb{C}^2$.

A necessary piece of the puzzle that takes us from S^3 to S^2 is a theorem stating that if G is a Lie Group and H is a closed Lie subgroup, there exists a projection π to the quotient G/H as a fibre bundle $(G, G/H, \pi, H)$ [3]. This is how we will go about defining the Hopf fibration, which is the proper name for the map $S^3 \to S^2$ that we have been using to move from spinors to physical states all this time. Our Lie group G is SU(2). Each element can be written as

$$U = \begin{pmatrix} \alpha & -\beta^* \\ \beta & \alpha^* \end{pmatrix}, \tag{27}$$

where the $\det U = 1$ condition translates to $|\alpha|^2 + |\beta|^2 = 1$. By our previous discussion of orthogonal spinors, this is equivalent to writing

$$U = \begin{pmatrix} u, v \end{pmatrix}, \tag{28}$$

where

$$u = \begin{bmatrix} \alpha \\ \beta \end{bmatrix}, v = \begin{bmatrix} -\beta \\ \alpha \end{bmatrix}$$

are orthogonal spinorsSince (u, v) and (v, u) are distinct and can be associated with u and v respectively, SU(2) matrices are one-to-one with spinors, confirming that SU(2) is isomorphic to S^3. But since we can quotient global phases out of spinors to get physical states, maybe we can do that here too! Choosing our closed Lie subgroup H to be the circle group U(1), careful application of Lie theory shows us that $(\mathrm{SU}(2), \mathrm{SU}(2)/\mathrm{U}(1), \pi, \mathrm{U}(1))$ is in fact a fibre bundle, where our projection π is a quotient map from our spinors in $S^3 \cong \mathrm{SU}(2)$ to $\mathrm{SU}(2)/\mathrm{U}(1)$ such that $|\psi\rangle \sim e^{i\theta} |\psi\rangle$. This means that SU(2) matrices aren't just transformations of spinors, they can represent spinors themselves! Rather than having separate states and transformations, we can just use SU(2) matrices to represent everything.

Thus, all our previous results for spinors can now be applied to SU(2) matrices. In particular, quotienting by U(1) sends the matrix U in Eq. (27) through the chain

$$\begin{pmatrix} \alpha & -\beta^* \\ \beta & \alpha^* \end{pmatrix} \mapsto [\alpha, \beta] \mapsto \begin{cases} \left[\frac{\alpha}{\beta} : 1\right] \mapsto \frac{\alpha}{\beta} & \text{if } \beta \neq 0 \\ [1 : 0] \mapsto \infty & \text{otherwise} \end{cases} \tag{29}$$

meaning we can associate each SU(2) matrix with an equivalence class in $\mathbb{CP}^1$ (i.e. a physical state) and a point on the Riemann sphere (i.e. a point on S^2). The quotient $\mathrm{SU}(2)/\mathrm{U}(1)$ is isomorphic to S^2, and since $S^3 \cong \mathrm{SU}(2)$, this means the fibre bundle projection

$$\pi : \mathrm{SU}(2) \to \mathrm{SU}(2)/\mathrm{U}(1) \tag{30}$$

is also a map

$$\pi : S^3 \to S^2, \tag{31}$$

Here, we have the general definition of the Hopf fibration. What makes all the setup we've done necessary is that the total space S^3 is not trivially $S^2 \times S^1$ (where we simply take the Cartesian product of the U(1) with the Bloch sphere). Globally, their topologies are different, so care needs to be taken when constructing the projection mapping.

We have finally come full circle, having arrived at the most general definition of the Bloch sphere (i.e. $\mathrm{SU}(2)/\mathrm{U}(1)$) for a spin-$\frac{1}{2}$ system, and having properly identified how the Hopf fibration is fundamentally responsible for our ability to associate spinors with physical states in a consistent way. Next time, we'll see much more of SU(2), properly analysing why it is the main group that transforms spinors and showing how it arises naturally when we identify rotations of S^2 with rotations of the Riemann sphere. Featuring examples that can be interactively plotted by readers at home, we will reveal the underlying structure connecting rotations to spinors, and finally explain why rotating physical states by a given angle only rotates the spinor by half the angle.

Bibliography

[1] Guido Fano and SM Blinder. *Twenty-first century quantum mechanics: Hilbert space to quantum computers*. Springer, 2017.

[2] Gareth A Jones and David Singerman. *Complex functions: an algebraic and geometric viewpoint*. Cambridge university press, 1987.

[3] Josh M. Lee. *Introduction to Smooth Manifolds*, volume 218 of *Graduate Texts in Mathematics*. Springer, 2012.

[4] Smite-Meister at Wikimedia Commons. Published under the Creative Commons Attribution-Share Alike 3.0 Unported license, note=Modified so the spin up and down states are labelled $|+\rangle$ and $|-\rangle$ instead of $|1\rangle$ and $|0\rangle$ respectively.

And that's it for yet another edition of Jeremy! Sorry if things got a bit *chaotic*. Hope it wasn't too *turbulent* (ok I'll stop now). Whether it was from an intro to Chaos in the weather or to your hearts, or in N-body systems, or even in friendly-looking pendulums, and much more, we hope you enjoyed this issue!

Don't forget to follow our socials, and contact us via **jeremy.physoc@gmail.com** for ideas, article submissions, or anything else really!
Catch you later everyone!

Website

@jeremy_usyd

Geocaching Puzzle

Cadigal Green is a place of multitudes - jaded engineers, canoodling couples, dogs(!), and one of the very few campus smoking areas. Make your way towards the Old School Building, but be careful not to trip on the boardwalk. Stay safe out there.

Guess the Rebus!

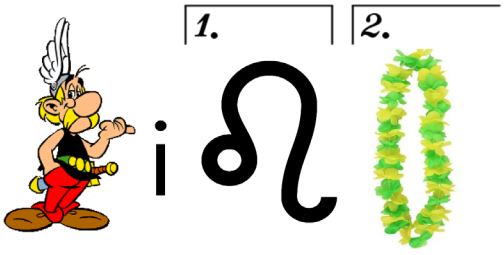

(Clue: Famous Physicist)

The detectives department at Jeremy has gained access to some golden archives of past Jeremy publications. Let us know if you are interested in past content and throwbacks, and we will include puzzles, articles, etc. in our future editions. Here are some samples to get you thrilled from Jeremy Issue 1, 2010!

Make sure to follow the Puzzle Society, who kindly gave us puzzles for this section

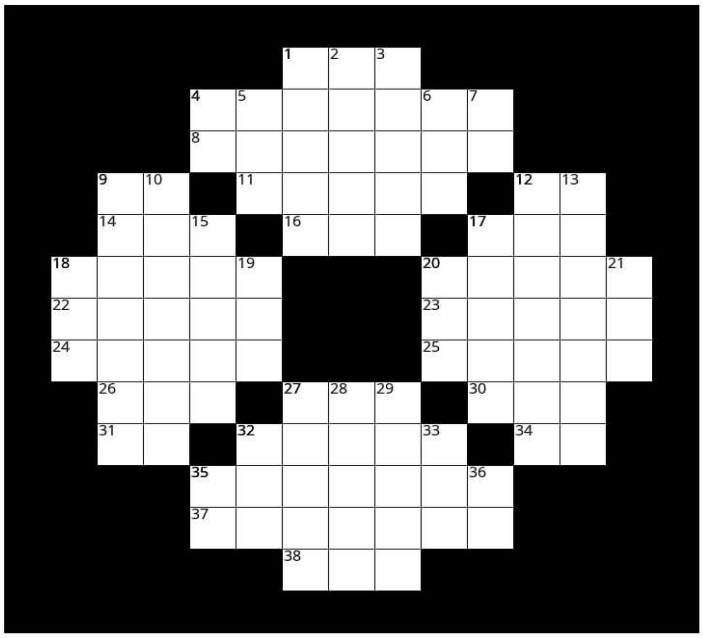

ACROSS

1. These could be stated by a scientist of the state
4. Those puzzles that you do frequently (Wordle, Strands, MinuteCryptic Etc.)
8. 26 Platforms
9. Contrary to popular belief, 1 of this is not 1 of whats in the name. Shocking!
11. You can threaten a child that they'll get these at Christmas
12. No 52 Perhaps?
14. Memes like doge / pepe
16. When youre being very much for real in text
17. Feature on Mars named for the pantheon (sans s)
18. Common safety principle around Ionising radiation
20. Some 10D have these
22. Parallel ones meet at infinity
23. Rousseau's most noted pedagogy
24. Where the LEGO Saturn V originated from
25. Fingers or numbers
26. Place to get fresh dough
27. The impulse response of a focused microscope
30. Most places drive on this (abr.)
31. Bread microbe, with consumption removed
32. Theres much hype about a unified theory of this
34. As with 12A, No 90
35. Releasing helium ones is banned in QLD
37. General term for an SCP
38. Exchanged for with tit

DOWN

1. It sounds like a cool as lizard, but its actually just bathroom matting :'(
2. Central feature of most churches
3. Erronius spin spell
4. Edisons controversial charge
5. Institution featured prominently in Oppenheimer (2023)
6. Method to quickly distribute information to TV's (and now phones) in a crisis
7. [Grain storage container] - [A moon of Jupiter]
9. Restful period of 24 hours that sounds motheaten
10. My violent evil monster just served us nachos (mnemonic)
12. First word to dont stop me now.
13. Can be a full one, or one of 3 other countries
15. The best kind of place for a proof to come from
17. Sleeping in madrid
18. The loser of the Fight of the Century
19. *guessing* makes an _ _ _ out of you and me.
20. A colour that you ought to be or die
21. Subject of Russel's paradox
27. S1E0 of a TV show is normally this
28. City in Alabama, famed in the Civil Rights movement
29. IEEE-754
32. A convex polygon can be divided into a _ _ _ of triangles
33. Figure toy, clipped short for space
35. If you're studying physics you're (probably) not graduating with this
36. American city where, famously 3 distinct types of rats have evolved in different areas of the city

Follow our socials
@usydphysoc
for the solution to the puzzles!

TRAVEL

Beyond the ordinary, one journey at a time